THESIS FOR DEGREE OF LICENTIATE OF ENGINEERING

Mesoporous Titania for High Rate Electrochemical Energy Storage

GIULIO CALCAGNO

Department of Chemistry and Chemical Engineering

CHALMERS UNIVERSITY OF TECHNOLOGY

Gothenburg, Sweden 2019

Mesoporous Titania for High Rate Electrochemical Energy Storage

GIULIO CALCAGNO

Licentiatuppsatser vid institutionen för kemi och kemiteknik
Chalmers tekniska högskola
Serie Nr 2019:20

Department of Chemistry and Chemical Engineering
Chalmers University of Technology
SE-412 96 Gothenburg
Sweden
Telephone + 46 (0) 31 772 28 12

Cover:
Mesoporous titania beads: from SEM image to asymmetric hybrid supercapacitor performance.

Printed by:
Chalmers Reproservice
Gothenburg, Sweden 2019

Mesoporous Titania for high rate electrochemical energy storage

GIULIO CALCAGNO
Department of Chemistry and Chemical Engineering
Chalmers University of Technology

ABSTRACT

Mesoporous titanium oxides are increasingly attracting interest as potential candidates for fast electrochemical energy storage. In this thesis, mesoporous titania of different polymorphs have been evaluated in relation to their ability to reversibly store Li^+ ions inside their structure. Mesoporous anatase beads with high crystallinity and specific morphology show high electrochemical capacity and high rate performance. The materials store charge through Li^+ ion insertion of both faradaic and extrinsic pseudocapacitive nature. Moreover, the discharge capacity retention after 150 cycles is >95%. On the other hand, ordered mesoporous titania, prepared via low-temperature spray deposition and mainly amorphous, shows a linear correlation between voltage and capacity, typical of an intrinsic pseudocapacitive material of insertion type. The material exhibits exceptionally high electrochemical capacity of 680 mAh g^{-1} during the first cycle, which, however, rapidly decreases over the following cycles. A combination of electrochemical and structural characterization techniques is used to study the charge/discharge behavior of the material and the origin of the irreversible capacity. X-ray absorption spectroscopy and energy-filtered TEM are carried out to analyse pristine and cycled samples in charged and discharged state. The results suggest that the irreversible loss in the capacity is due to the formation of electrochemically inactive phases mainly located at the surface of the material. Additionally, electrodes based on mesoporous anatase beads are paired with a commercial activated carbon electrode that presents a broad distribution of mesopores and very high surface area to design a hybrid asymmetric supercapacitor. The device shows extraordinary stable performance with energy densities of 27 Wh kg^{-1} at the relatively fast discharge current of 2.5 A g^{-1} for 10 000 cycles and high power densities during fast cycling.

Key words:

Mesoporous Titanium Dioxide, Pseudocapacitance, XAS, Hybrid Asymmetric Supercapacitors

List of publications

1. Electrochemical and structural characterization of lithiation in spray deposited ordered mesoporous titania as anode for Li ion batteries
   Gunnar Símonarson, Giulio Calcagno, Antiope Lotsari, Anders E.C. Palmqvist
   Submitted for publication
2. Towards fast charging negative electrodes for hybrid asymmetric supercapacitors using anatase TiO_2 beads
   Giulio Calcagno, Anders E.C. Palmqvist, Alan Dang, Aleksandar Matic and Carmen Cavallo
   Manuscript

Contribution report to the listed publications:

1. Responsible for electrochemical measurements and jointly responsible for XAS and TEM measurements and writing the manuscript.

2. Responsible for experimental work and writing the manuscript.

List of abbreviations

AC: activated carbon

BET: Brunauer, Emmett and Teller

BJH: Barret, Joyner and Halenda

CV: cyclic voltammetry

EC-DMC: ethylene carbonate and dimethyl carbonate

EDLC: electric double layer capacitor

EFTEM: energy filtered transmission electron microscopy

GCD: galvanostatic charge discharge

GCPL: galvanostatic charging with potential limitation

HASC: hybrid asymmetric supercapacitor

HDA: 1-hexadecylamine

HESS: hybrid energy storage system

LIB: lithium ion batteries

LP30: 1M $LiPF_6$ in 1:1 EC-DMC

MS: multiple scattering

NEXAFS: near edge x-ray adsorption fine structure

NMP: N-methyl-2-pyrrolidone

PSC: pseudocapacitor

PVDF: polyvinylidene fluoride

SC: supercapacitor

SEI: solid electrolyte interphase

SEM: scanning electron microscope

TEM: transmission electron microscope

TIP: titanium (IV) isopropoxide

XAS: X-ray absorption spectroscopy

Table of Contents

1. INTRODUCTION

The growth of societal energy requirements, the depletion of resources and the increased pollution require the transition to renewable energy alternatives. In 2018 the global electricity consumption had reached ~23 000 TWh, of which only ~538 TWh was produced through solar and wind technologies.[1] To efficiently use these energy sources, which are inherently intermittent, and increase their contribution to the total energy mix, advanced energy storage systems must be developed.[2,3]

The increased interest in the large market of electrification foresees a huge challenge for electrochemical energy storage development and especially from a materials perspective. It is essential to consider the need for greener chemistry and the concern over long term abundance of materials. When exploiting elements like nickel and cobalt, their shortage and possible geopolitical issues must be taken into account. Therefore, research has focused on more abundant elements like titanium, iron and manganese.[4,5] Titanium oxide, for example, is one of the promising material candidates because it is very abundant in Earth´s crust, it is chemically stable, it is characterized by low toxicity and its production has typically a low cost. In addition, titanium oxide is a suitable material for storing energy by inserting lithium ions in its structure, which is the basic storage mechanism of Li-ion batteries (LiBs).[6]

Among the different energy storage systems, Li-ion batteries (LiBs) have attracted worldwide attention due to their versatility and relatively low cost. They are used in a wide range of applications, like portable electronics, electric vehicles and grid applications. This is due to their ability to store energy with high gravimetric density (commercially between 150 to 300 Wh kg^{-1}) through the intercalation/insertion of Li^+ ions in their electrodes. However, they are not suited for applications requiring high power densities, due to their slow chemical processes, also called faradaic processes.[7,8] On the other hand, supercapacitors (SCs) are devices showing high power capability, great stability but low energy density, with commercial supercapacitors providing ~5 Wh kg^{-1}. They store energy through the physical separation of charges at the surface of electrodes, forming an electrical double layer (EDL). This storage mechanism is typically called EDL capacitance.[9]

In the last years, new applications requiring performance in between Li-ion batteries and supercapacitors have arisen. One alternative to approach this challenge efficiently is by hybrid asymmetric supercapacitor (HASC), combining battery and supercapacitor electrodes in tandem. Li-ion HASCs aim at achieving both high power and energy densities by using a carbon EDL material as positive electrode coupled with a Li ion intercalation negative electrode. A proper design

of the electrodes is necessary to balance the different charge storage mechanisms and optimize the performances.[10,11]

The technological frame is even more complex when you consider that new applications have heavier energy demands, which means that new materials with improved electrochemical performance are required. Nanomaterials chemistry can provide a solution by the development of materials surpassing the limitation of the typical bulk materials. Nanosized materials have shown to store a large amount of energy and enable its rapid and efficient release.[12] Among this class of materials, mesoporous nanostructured materials are particularly interesting because of their high surface area, offering more lithium insertion channels, pore pathways for fast diffusion of the Li ions and good accommodation of strains.[13] The proper choice and design of nanostructured materials represent a viable path towards a more sustainable and efficient electrochemical energy storage.

In recent years, a peculiar electrochemical energy mechanism has attracted the researchers' interest. Pseudocapacitance, where pseudo- means "not actually but having the appearance of", refers to fast charge transfer faradaic reactions proceeding at the surface of some materials, like ruthenium oxide, with an electrochemical signature similar to a capacitance.[14] This type of pseudocapacitance is defined as intrinsic. In addition, it has been demonstrated that nanosizing transition metal oxides with layered crystalline structure, like crystalline titanium oxide, can give rise to an extrinsic pseudocapacitance of insertion type. This particular behavior is shown when the material size is reduced to the nanometer level and the Li^+ ion insertion proceeds at the surface via fast charge discharge kinetics.[15,16] Electroactive materials characterized by pseudocapacitive properties constitute promising candidates as electrodes for Li-ion HASCs.

Mesostructured titanium oxide seems to possess the right set of properties to be one of the materials for high power electrodes for future storage applications. Furthermore, different titania polymorphs show different electrochemical mechanisms. For example, amorphous titania has recently demonstrated intrinsic pseudocapacitive performance.[17,18,19]

The objective of this thesis is to study the lithium insertion/extraction mechanisms into two mesoporous titania materials prepared in our laboratories and how different structures affect the electrochemical signature. Specifically, we compare i) microsized mesoporous anatase beads and ii) ordered mesoporous titania composed of a mixture of anatase nanocrystals and amorphous titania. We show that a combination of electrochemical and structural characterization is fundamental to fully understand the storage mechanism. Moreover, the thesis presents also the performance of a hybrid asymmetric supercapacitor comprising a negative electrode based on mesoporous anatase beads and a commercial activated carbon as a positive electrode.

2. BACKGROUND

2.1 Electrochemical Energy Storage

Systems for electrochemical energy storage and conversion include batteries, fuel cells, and supercapacitors. Although the energy-providing processes take place at the phase boundary of the electrode/electrolyte interface in all of the three systems, they show different mechanisms and therefore different performance. Fuel cells are promising devices for clean energy storage, because they use hydrogen as energy source and are characterized by high energy densities. This thesis will not cover these devices. In Figure 1 a Ragone plot is used to compare the performance of the three different systems in terms of energy density and power density.

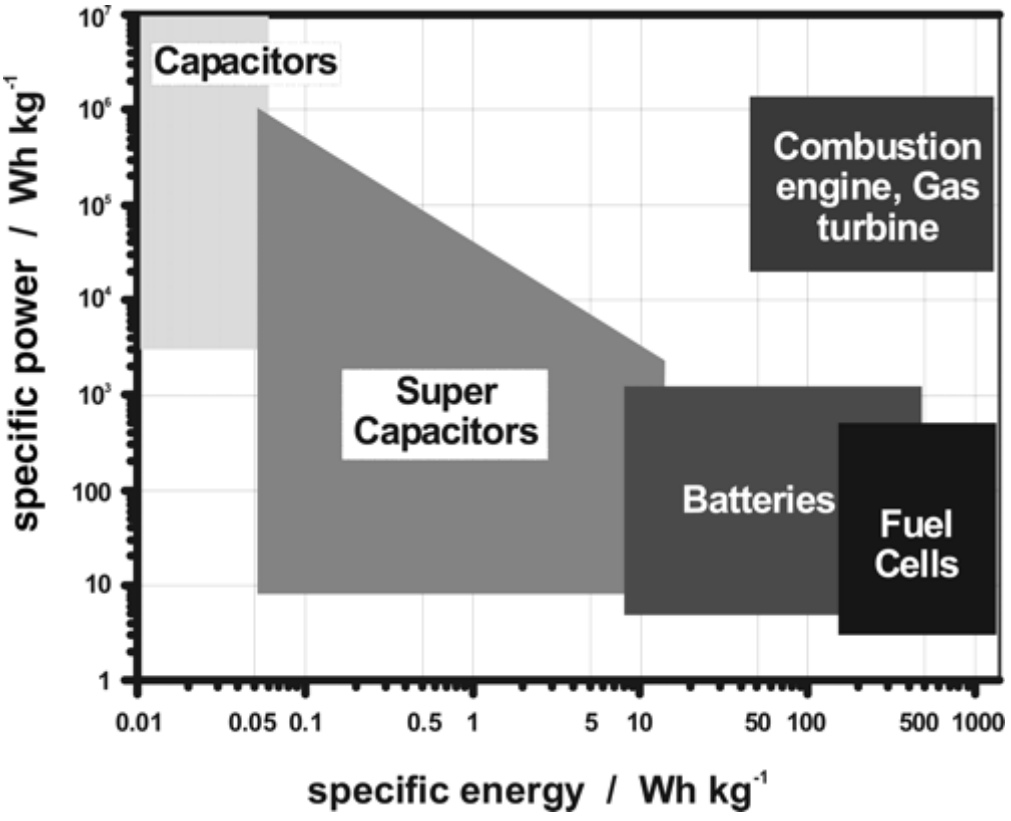

***Figure 1**: Simplified Ragone plot representing the performance areas for the different energy storage systems in comparison to combustion engines. Reproduced with permission from (8).*

2.2 Batteries

Batteries have been in use for over two centuries, dating back to 1800 and Alessandro Volta in Como, Italy. There are three general classes: primary batteries that are discharged once and discarded; secondary rechargeable batteries that can be discharged and then restored to their original

condition by reversing the current flow through the cell; and specialty batteries that are designed to fulfil a specific purpose. Simply stated, a battery is composed of two electrodes, an electrolyte, a separator and current collectors. Electricity is generated by conversion of chemical energy via redox reactions at the anode and cathode. As the reaction at the anode usually takes place at lower electrode potentials than at the cathode, the terms negative and positive electrode are used. The negative electrode is a good reducing agent (electron donor) such as lithium, zinc or lead. The positive electrode is an electron acceptor such as lithium cobalt oxide, manganese dioxide, or lead oxide. The electrolyte is a pure ionic conductor that physically separates the anode from the cathode. The specific capacity of a battery, expressed in the following in mAh g^{-1} is the total amount of electrical charge Q that can be drawn from the device before a specified cutoff voltage V is reached; the specific energy, expressed in mWh g^{-1} or Wh kg^{-1}, is used to assess the energy content of the system, whereas the specific power, expressed in mW g^{-1} or W kg^{-1}, is used to assess the rate capability.[20]

2.2.1 Li-ion batteries (LiBs)

In the field of secondary batteries, lithium has long received much attention as a promising anode material, due to its lowest electro-negativity (-3.0 V Vs standard calomel electrode) and light weight.[21] In 1970s Whittingham proposed the idea of rechargeable lithium batteries and developed a prototype that used a lithium-metal as anode.[22] The battery had a high energy density and the diffusion of lithium ions into the cathode was reversible, making the battery rechargeable. However, needle-like lithium crystals, called dendrites, grow on the anode upon cycling, leading to short circuits and fires. In the late 1970s and early 1980s, Goodenough developed rechargeable batteries with cathodes made from layered oxides capable of storing lithium ions.[23] This greatly improved the energy density, and lithium cobalt oxide remains the cathode material of choice for the LiBs commercially available. The breakthrough in the 1980s, which lead to the lithium ion battery concept, was made by Yoshino who exploited an old concept of using carbonaceous materials as anode intercalation host.[24] In the charged state, lithium is now in ionic form thus avoiding dendrite formation. For their discoveries and the fundamental contribution to the development of lithium ion batteries, the three scientists have been granted the Nobel Prize for Chemistry in 2019. Later on, Dahn and co-workers published their report on the principle of lithium intercalation in graphitic anodes and the fomation of a protective film due to electrolyte decomposition. They adopted a model developed earlier by Peled to describe the passivation on lithium metal and named this surface film on carbonaceous anodes as “solid electrolyte interface” (SEI). It has been generally agreed that the electrolyte reduction products are the main components of an SEI and dictate the chemical as well as thermal properties of the electrode.[25] Graphite is a cheap and stable negative

electrode material, but its specific capacity is not so high, with a theoretical limit of 372 mAh/g. Furthermore, the insertion of Li^+ ions inside the graphite structure is diffusion controlled and consequently relatively slow.[26] To improve the energy density and the cycling rate capability, many alternatives to graphite, like silicon, tin, germanium and transition metal oxides have been extensively explored.[27,28,29] In general, the next generation anodes and cathodes require: i) to effectively and reversibly host Li providing high capacity, ii) having good electronic and ionic conductivity, iii) allowing for fast kinetics, and iv) showing high mechanical stability upon volume change during cycling. Research and engineering are also focused on developing better binders, separators and current collectors. [4] Figure 2 reports a schematic depiction of a Li-ion battery.

Nowadays, the best performing Li-ion batteries in the market delivers ~300 Wh kg^{-1}. A recent report from EUCAR, the European Council for Automotive R&D, identifies in 450 Wh kg^{-1} the energy goal of next generation batteries for electric car, to be reached by 2030.[30] In terms of power density, Li ion batteries dominate the field of applications requiring more than 20 min charging/discharging time.

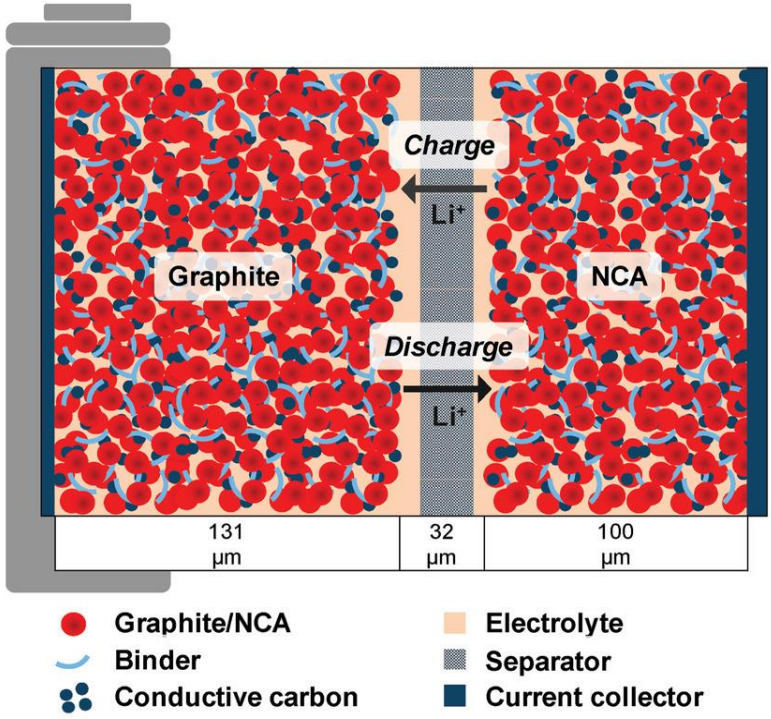

***Figure 2**: Schematic depiction of a typical 18650-type cell for an LIB system with an NCA cathode (LiNi0.8Co0.15Al0.05O2), a graphite anode, and an organic carbonate solvent-based electrolyte ($LiPF_6$ in EC: DMC). Reproduced with permission from (47).*

2.3 Supercapacitors

The discovery of the phenomenon of storing an electrical charge on surfaces arose from experiences associated with the rubbing of amber already in ancient times. The principle that electrical energy can be stored between two metallic plates, separated by an insulator, is known since the late 18th century. A device able to store electricity in this way is called capacitor and it stores an energy $G = ½ CV^2$, with G being the Gibbs free energy and C the capacitance (expressed in Farad, F), due to a voltage difference V between two plates accommodating charge +q and -q. An electrochemical capacitor is composed of two electrodes and an electrolyte that works as an insulator. At the surface of the two electrodes, one of which is charged negatively with respect to the other, charge separation and storage occur. Historically, the electrochemical capacitors were called supercapacitors to differentiate them from the capacitors, because of the much higher capacitance they were able to store. There are two main classes of supercapacitors: electric double layer capacitors (EDLC) and pseudocapacitors.[31]

2.3.1 Electric double layer capacitors (EDLC)

EDLCs are the most common and commercially available supercapacitors, therefore many reviews on EDLCs and materials can be found in literature.[32] The charge is stored through a physical process of adsorption of ions at the interface between electrodes and electrolyte, forming a double layer of charges, as depicted in Figure 3. The accepted theoretical model of the electric double layer is based on the works of Helmholtz, Gouy and Chapman, Stern and Grahame.[33,34,35] The double layer in this model is described as composed of a diffuse layer, towards the solution, and a compact layer, next to the surface, where partial desolvation of the ions occurs. The electrode materials in an EDLC possess a very high surface area, as the specific capacitance is directly proportional to the accessible surface area. Typically, the electrodes are made of carbon-based materials with high porosity and broad distribution of pore size.[36] The commercially available supercapacitors usually comprise two electrodes both made of activated carbons and are defined symmetric for this reason. Electrolytes can be aqueous, with operating voltages limited by water decomposition, organic, the most common being acetonitrile, and more recently ionic liquids.[37] Recent findings have claimed the importance of microporosity to achieve high specific capacitance, which is why carbon nanomaterials of different form have been extensively studied.[38] Typical devices can store energy in the range of 5 Wh kg^{-1} and reach powers of several kW. EDLCs dominate the applications requiring a charging/discharging time in the time scale of seconds.

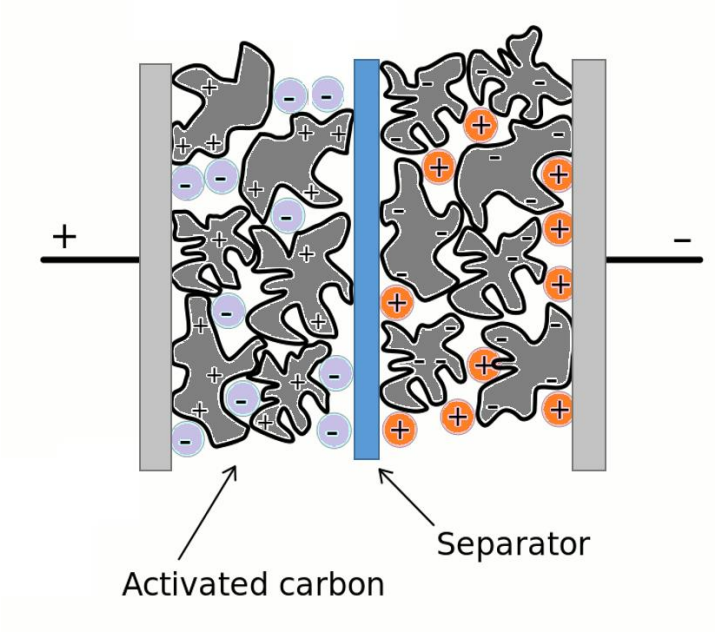

***Figure 3**: Schematic depiction of a typical symmetric supercapacitors and the formation of an electric double layer of charges at the interface between of electrolyte and electrodes' surface.*

2.3.2 Pseudocapacitors

Pseudocapacitors (PSCs) represent the second class of supercapacitors. Pseudocapacitance refers to fast charge transfer faradaic reactions happening at the surface of some materials, like ruthenium oxide, with an electrochemical signature similar to a capacitance. In his influential book regarding Electrochemical Capacitors, Conway stated: "Pseudocapacitance… is faradaic in origin, involving the passage of charge across the double layer, as in battery charging and discharging, but capacitance arises in account of the special relation that can originate for thermodynamic reasons between the extent of charge acceptance Δq and the change in potential ΔV, so that the derivative $d(\Delta q)/d(\Delta V)$, which is equivalent to a capacitance, can be formulated and experimentally measured by dc, ac or transient techniques".[31] To summarize, fast redox reactions exhibiting a linear dependence of the charge stored with the width of the potential window. Pseudocapacitance holds the promise of achieving battery level energy density, however typical pseudocapacitive materials show limited cycling ability.

The electrode material for PSCs can be very diverse but two main classes can be defined: metal oxides and conducting polymers. Metal oxides like RuO_2, MnO_2, V_2O_5 and Nb_2O_5 have been extensively studied.[39,40,41,42] RuO_2 is a good performing material, but has a very high cost, while MnO_2 and V_2O_5 suffer from poor conductivity and/or cycling stability. Nb_2O_5 has recently shown promising performance and good stability, especially when in combination with a carbon matrix. Conductive polymers, like polyaniline and polythiophene, generate capacitance by redox

reactions.[43,44] Because of swelling and shrinking during cycling, the polymers suffer from low cycling stability.

Pseudocapacitance can also occur when nanosizing transition metal oxides with layered crystalline structure giving rise to another phenomenon, called intercalation pseudocapacitance.[15,16] Intercalation/insertion pseudocapacitance occurs when ions intercalate/insert into the layers or tunnels of the transition metal oxide and undergo charge transfer and change of metal valance, with no or limited crystallographic change. Limited phase change means that just a very small volume modification happens between the charged and discharged state. Being a surface limited process, the intercalation/insertion pseudocapacitance is very interesting for high rate capability applications, thanks to fast ion transport kinetics and long stability. The fast surface kinetics is the main characteristic differentiating this phenomenon with diffusion limited battery intercalation. Moreover, two types of this mechanism have been discovered: intrinsic pseudocapacitance, which is an inherent property of the material, so it is displayed in a wide range of particle sizes and morphologies, and extrinsic pseudocapacitance, which emerges when the material is nano-engineered and the surface/volume ratio is increased. TiO_2, $LiCoO_2$ and Li_4TiO_4 are very good examples of this phenomenon.[45,46]

2.4 Hybrid Supercapacitors

In the last years, new applications requiring performance in between Li-ion batteries and supercapacitors have arisen. These intermediate devices need to store tens of Wh kg^{-1} with discharging time between several seconds up to 30 minutes. One way to address this challenge is by combining the mechanisms of faradaic, pseudocapacitive and capacitive storage. In the literature different terminology has been used to define a series of devices characterized by the combined storage mechanisms. In this thesis, the term “hybrid” will be used to describe the class of all these devices. Examples of hybrid supercapacitors are asymmetric supercapacitors, which are one of the main topics of this work, and redox enhanced EDLCs, which contain additives in the electrolyte that undergo surface redox reactions on the carbon electrode surface.[47,48]

2.4.1 Asymmetric supercapacitors

Asymmetric refers to the use of different positive and negative electrodes, typically one battery-type and the other supercapacitor-type. The use of two different electrode materials can extend their operating voltage window beyond the thermodynamic decomposition voltage of electrolytes. This is especially important for aqueous electrolyte, where the operating voltage has been extended beyond 2.0 V.[49]

The extension of the operating voltage can improve substantially the specific energy because the latter is proportional to voltage squared. It is also important to notice that to guarantee a charge balance during operation and optimal performance, the mass ratio of the two electrodes should be adjusted, considering the different storage mechanisms.

In addition, when evaluating the performance of these systems, it is important to state clearly which component is included in the calculation of the values of energy and power density. Energy densities expressed as a function of the active material are misleading and far from the device performance.[50,51]

Among the different types of asymmetric supercapacitors, Li-ion HASCs have received a lot of attention. They consist of a Li-ion intercalation negative electrode coupled with an EDLC carbon electrode, both immersed in a non-aqueous Li-containing electrolyte.[52,53] The first prototype of this device was reported by Amatucci et al. in 2001, and it was combing an activated carbon electrode with a lithium titanate electrode (nowadays used for power batteries as replacement of graphite) both immersed in the standard Li-ion battery electrolyte.[54]

In **Paper 2**, we present a slightly different version of this configuration, where the battery electrode store charge via a pseudocapacitance of insertion type mechanism. This type of Li-ion HASC is very promising because it combines the increase in specific energy of a hybrid device with the high rate capability of pseudocapacitance.

Figure 4 reports a representation scheme of a SC, a Li-ion battery and a Li-ion HASC, which is a direct combination of the first two devices.

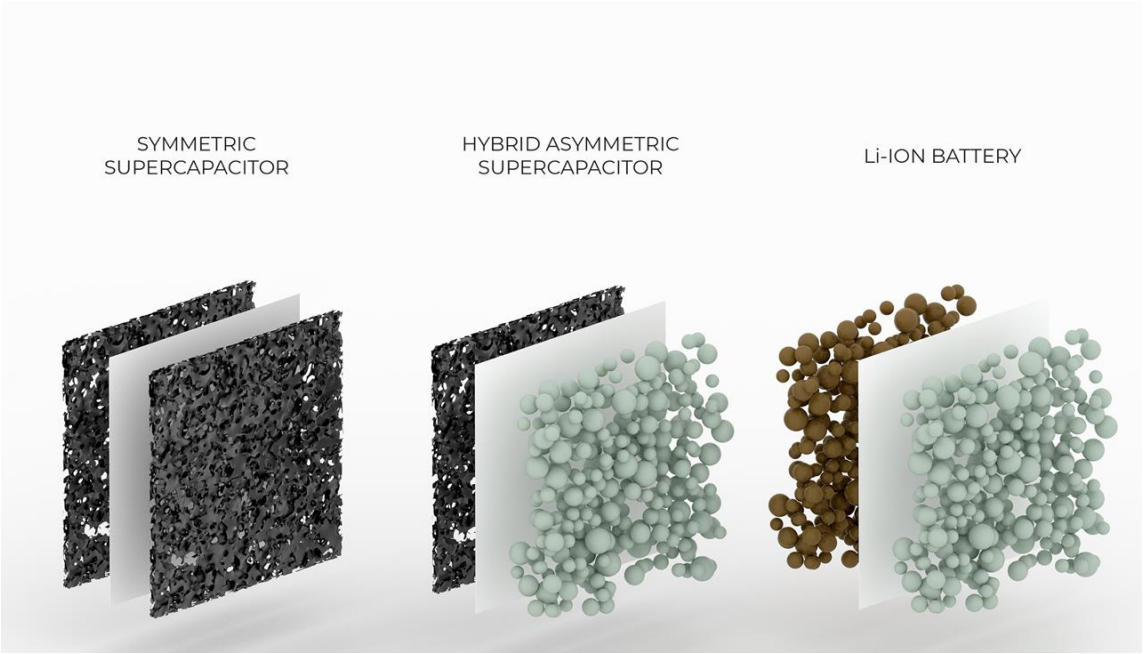

Figure 4*: From left to right: Symmetric Supercapacitor (SC), Hybrid Asymmetric Supercapacitor (HASC) and Li-Ion Battery.*

2.5 Titanium dioxide

Titanium dioxide, or titania, is in its crystalline form semi-conducting with a wide band gap composed of two earth abundant elements, titanium and oxygen. More than 80% of the titania global production is used as pigment in paint, plastics and paper and in form of thin films. Other applications are in cosmetics, ceramics and textiles. Thanks to its peculiar electrochemistry, nanostructured titania has been studied and applied in various energy and environmental applications, including solar cells, water and air purifications, self-cleaning surfaces, photoelectrochemical cells and electrochemical energy storage.[55]

2.5.1 Polymorph structures

Crystalline titania is naturally present in the form of three crystalline polymorphs: rutile (tetragonal), anatase (tetragonal) and brookite (orthorhombic). Of these, rutile, the most common in nature, is the thermodynamically stable phase under ambient conditions, with both anatase and brookite being metastable with respect to rutile.
The basic unit-cell structures of these phases are shown in Figure 5.[56]

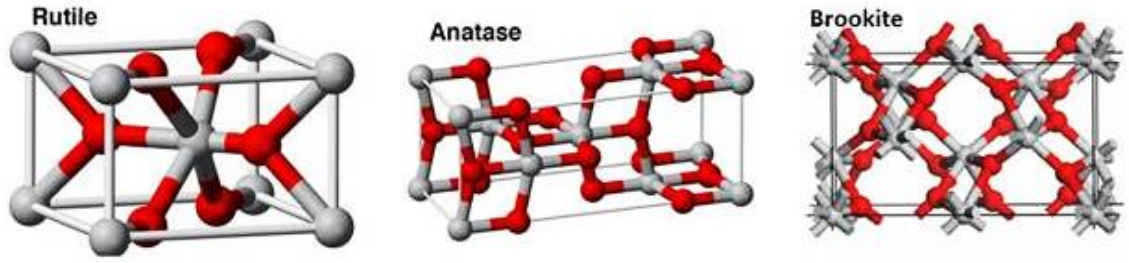

Figure 5*: Crystal structures of rutile, anatase and brookite titanium dioxide.*

Anatase is tetragonal containing 12 atoms per unit cell and each Ti atom is octahedrally coordinated to six O atoms and each O atom is coordinated to three Ti atoms. In both cases, the TiO_6 octahedron is slightly distorted, with two Ti-O bonds slightly greater than the other four, and with some of the O-Ti-O bond angles deviating from 90°. This coordination leads to the presence of octahedral and tetrahedral interstitial sites. Another phase called TiO_2 (B) (monoclinic) is produced by hydrolysis of $K_2Ti_4O_9$ followed by heating. Low temperature production of titanium dioxide gives rise to an amorphous polymorph. Previous studies of the amorphous polymorph have shown that its structure is composed of an anatase core like with defects near the surface.[57,58]

2.5.2 TiO_2 as anode in LiBs

Titanium dioxide is a valid alternative to graphite as anode material for LiBs. This is due to its high abundance, low toxicity and cost and structural stability during Li ions insertion/extraction. The electrochemical signature of TiO_2 depends on the polymorph, particle size and morphology. [59,60,61,62] Anatase and rutile insert Li ions reversibly according to the Equation (1),

$$TiO_2 + xLi^+ + xe^- \leftrightarrow Li_xTiO_2 \quad (1)$$

where *x* ranges between 0 and 1. Following the insertion process of Li^+ into titania, three regions can be described. In the first region, at low concentration of Li, a solid solution is formed. The second region is associated to the redox process in (1) where half of the octahedral sites are filled and TiO_2 and Li_xTiO_2 co-exist due to a phase separation. The theoretical specific capacity of lithium insertion into anatase is 335 mAh g^{-1} and it corresponds to the composition Li_1TiO_2 reached at the end of the third region when the filling of the last octahedral sites is completed.[63] TiO_2 (B) and amorphous titania instead are characterized by pseudocapacitive performance.

Unfortunately, titania electrodes are typically showing capacities between 150 to 200 mAh g^{-1} due to the slow Li diffusion and the effect of production parameters (like annealing, presence of water and morphologies).[64,65] Nanostructuring the materials has been shown as one strategy to enable the rapid and efficient storage and release of energy. One, two and three dimensional TiO_2 structures have been extensively studied, showing that nanoengineering is an efficient way to improve the Li storage properties into the titania structure.[66,67,68,69] Mesoporous morphologies in particular have shown very high energy densities and the best rate performances reported. Mesoporous nanostructured materials are interesting because of their high surface area, offering more lithium insertion channels, structured pore pathways for fast diffusion of the Li^+ ions and good accommodation of strain.

Doping of the structure and formation of composite with carbon are the other strategies followed by researchers to improve the titanium dioxide electrochemical performance.[70]

3. EXPERIMENTAL METHODS

3.1 Synthesis of the materials

3.1.1 Mesoporous anatase TiO_2 beads

Titanium (IV) isopropoxide (TIP) (97+%), ammonium hydroxide solution (30−33%), Potassium Cloride (KCl) (99.99%, trace metal basis) and 1- hexadecylamine (HDA) (technical, 90%) were purchased from Sigma Aldrich. All the chemicals were used as received. Synthesis of mesoporous anatase TiO_2 microbeads were prepared by controlled hydrolysis of TIP in hydroalcoholic medium for 18 h with HDA as a structure-directing agent and KCl to regulate ionic strength, followed by autoclaving at 160 °C in hydroalcoholic ammonia for 16 h and calcining at 500 °C for 2 h in air of the obtained solid.[71]

3.1.2 Mesoporous amorphous TiO_2

Spray deposited ordered mesoporous titania was synthesized using a method previously reported.[72] In short, a reaction solution was prepared by stirring 3 g ethanol (99.5%, Solveco), 2.25 g block co-polymer Pluronic™ F127 (Sigma Aldrich) and 1.5 g 5 M HCl (Sigma Aldrich) in a closed polypropylene bottle until the F127 was completely dissolved. Subsequently, 1.5 g titanium butoxide (97%, Sigma Aldrich) was added to the solution and the solution was stirred for approximately 10 minutes, until the titania precursor was dissolved. The final molar composition of the reaction solution was (titanium butoxide:ethanol:HCl:water:F127) (1:14.8:1.57:15.7:0.041). The solution was stored for three hours at 40 °C in the closed polypropylene bottle. The reaction solution was spray deposited (15 second spray time) on glass slides (VWR 631-1551, 76x26 mm) using an Aztek A470 Airbrush, with a 0.30 mm general purpose nozzle (Aztek 9305 CX). After deposition, the film was aged for 72 hours in a closed climate chamber at 75 % relative humidity (RH). Subsequently, the films were exposed to UV irradiation for 24 hours to photocatalytically remove the F127 polymer template. The ordered mesoporous titania material was collected by scraping the film of the glass slides. Titania anatase nanoparticles of ~15nm diameter (Alfa Aesar, product number 45603) were used as a reference.

3.2 Electrode fabrication

Electrodes were prepared by mixing the mesoporous titanias with carbon black, Super-P™ (Alfa Aesar), and Kynar® PVDF binder (Arkema) in NMP (N-methyl-2-pyrrolydone, anhydrous, 99.5%, Sigma Aldrich) and finally deposit the mixture on a copper current collector. First, mesoporous anatase beads were mixed by ball milling at 10 Hz for 10 minutes in a ZrO_2 coated cup with ZrO_2 balls in a Retsch MM400 ball mill. The ball milled mixture was transferred to a glass vial and Super-P™ and Kynar® 5% (w/w) solution in NMP was added. The solution was stirred overnight in a capped vial, forming a slurry having a weight ratio of (TiO_2:Super-P:PVDF) of (8:1:1). The slurry was coated onto a copper foil through a TQC AB3400 motorized automatic film applicator. A stainless-steel doctor blade (Wellcos Co.) was used to coat a 150 µm thick coating of the slurry. The as prepared electrode was let dry overnight at room temperature with further additional drying at 80 °C for 2 hours to let the NMP completely evaporate.

In Paper 2, the activated carbon electrodes (~10 mm diameter, ~300 µm, ~12 mg/cm^2 active material) were prepared following a procedure reported in literature.[73] In summary, PTFE binder (60 weight % aqueous dispersion), acetylene black conductive additive (Vulcan® XC72R) and Kuraray YP 50F activated carbon were mixed in ethanol. The resulting material was rolled with a PTFE rolling pin and folded over itself 5-10 times until a single freestanding film was formed. This film was dried overnight at 160 ºC in air, ground into a powder through mesh sieve, and then dried again under high vacuum at room temperature. The resulting electrode material contained activated carbon, carbon black conductive additive, and PTFE binder in a 90:5:5 mass ratio, respectively. Freestanding 10 mg electrode pellets were pressed from the powder in a 1 cm die hydraulic press under an applied uniaxial force of 2 tons.

3.3 Device fabrication

In both **Paper 1** and **Paper 2**, the electrodes were studied as anode in half Li-ion cell. The electrodes (~10 mm diameter, 2 mg cm^{-2} active material) were transferred to a glove box (H_2O and O_2 less than 1ppm) and dried under vacuum at 80°C in a Buchi oven. Coin cells were assembled in an argon-filled glovebox using CR2032 housings. Glass microfiber was used as separator, soaked with 60 µL of electrolyte commercial LP30 solution while lithium metal disc was used as anode (~11 mm, 4 mg cm^{-2}). The hybrid asymmetric supercapacitors were built similarly as coin cells, using the mesoporous anatase electrode as negative electrode (battery-type) and Kuraray YP 50F activated carbon as positive electrodes (capacitor-type).

4. ANALYTICAL TECHNIQUES

4.1 Structural characterization

The structural characterization of the materials was performed through scanning electron microscopy (SEM), transmission electron microscopy (TEM), X-ray absorption spectroscopy (XAS), X-ray diffraction (XRD) and Nitrogen Sorption.

4.1.1 Scanning electron microscopy (SEM)

SEM is a non-destructive microscopy technique operated in ultra-high vacuum. The sample is scanned by an electron beam generated thermo-ionically by an electron gun. The irradiated sample emits secondary and back scattered electrons, which provide information about the surface topography and the surface composition respectively. In **Paper 2**, the morphology of the anatase TiO_2 beads was investigated by JSM 7800F scanning electron microscope (SEM).

4.1.2 Transmission electron microscopy (TEM)

TEM is also a non-destructive microscopy technique. The electron beam, at high accelerating voltages, interact with the sample and pass through it, forming a projection of the structural features on a detector placed underneath. Being a transmission technique, it requires very thin samples, with thicknesses in the order of 50 to 100 nm. Bright field (BR) and High resolution (HR) TEM was used in this work. To obtain compositional maps of the samples, energy filtered (EF) experiments can be performed. In **Paper 1**, TEM samples were prepared by a TEM lamella lift-out technique in a FIB/SEM. The lamella was attached to a copper half grid and was ion thinned to transparency in the FIB/SEM. The TEM observations were performed on a FEI Tecnai G2 operating at 200kV and on a FEI Titan operating at 300kV. Energy filtered EFTEM experiments were performed on the Titan.

4.1.3 X-ray diffraction (XRD)

X-ray diffraction is the most used technique to study crystalline materials. When a crystalline material is irradiated with a monochromatic X-ray beam of wavelength λ, part of the X-rays will be diffracted following the Bragg´s law: $n\lambda = 2d\sin\vartheta$, where d is the distance between the crystalline planes and 2ϑ is the angle between the incoming and the outgoing beams. The resulting diffraction pattern, characterized by the so-called Bragg peaks, is specific for a crystal structure.

In **Paper 2**, The crystallinity of the mesoporous anatase beads was studied with powder X-ray diffraction (XRD) and an X'Pert Pro diffractometer (Cu Kα radiation, λ = 0.154184 nm) equipped with an X'Celerator ultrafast RTMS detector. The angular range was 10-90° (in 2θ) and the angular resolution (in 2θ) was 0.001°. A 0.04 rad soller slit, a 1° divergence slit, and a 20 mm mask were used on the incident beam path, while a 6.6 mm antiscatter slit and a 0.04 rad collimator were used on the diffracted beam path. By using the MAUD software package, the Rietveld analysis of the obtained patterns was performed.[74]

4.1.4 X-ray absorption spectroscopy (XAS)

When a sample is exposed to an x-ray radiation, the electric field of the radiation will interact with the bound electrons of the material. At specific energies, this interaction will be of adsorption type and result in a photoexcitation process. By studying the energy of the ejected photoelectrons, X-ray absorption spectroscopy is used for determining the local geometric and/or electronic structure of matter. It is specifically useful to study amorphous materials, which cannot be studied via diffractive techniques. In **Paper 1**, X-ray absorption measurements on pristine, cycled and reference samples were performed at the Balder XAS beamline of the MAX IV synchrotron in Lund, Sweden.[75] The measurements were carried out in transmission mode and titanium foil was used as a reference for energy calibration of the spectra. XAS measurements were performed on the samples that were cycled to the previously defined cutoff voltages. After 50 cycles of charge/discharge the cycling was interrupted at 2.9 V which corresponds to the total deintercalation of the reversibly stored Li. Additionally, a sample was prepared by interrupting the cycling at 0.7 V after 50 cycles, corresponding to the highest intercalated state studied here. To prevent the samples from reacting to oxygen or other species in the environment before the measurement, the samples were prepared in an argon filled glovebox with H_2O and oxygen concentration < 1 ppm. First, the cell was opened, and the electrode was rinsed with DMC (~300 µL) and let to dry. To remove the sample from the copper current collector a piece of Kapton tape was applied on top of the electrode and removed, leaving the sample attached to the tape. Subsequently, the tape was folded to isolate the sample before it was moved out of the glovebox.

4.1.5 Nitrogen Sorption

Nitrogen sorption is a technique used to evaluate the specific surface area, the pore size, pore volume and pore size distribution of a material, through the adsorption of nitrogen on the surface. The nitrogen adsorption begins with the adsorption of a monolayer which allows, by using the teory of Brunauer – Emmett – Teller (BET), to calculate the specific surface area. By increasing the

nitrogen partial pressure inside the pores, the phenomenon of capillary condensation occurs which leads to a rapid increase of the amount of nitrogen adsorbed. This area of the nitrogen sorption isotherm is used to measure the pore size/volume and pore size distribution following the method of Barret - Joyner - Halenda (BJH). In **Paper 2**, N_2 adsorption and desorption isotherms were recorded at -196 °C using a Micromeritics Tristar instrument. The pore volume and size distribution were determined from the adsorption isotherm and the BJH method and the specific surface area was calculated by the BET multipoint method.

4.2 Electrochemical Characterization

4.2.1 Cyclic voltammetry (CV)

Cyclic voltammetry is one of the linear sweep voltammetry techniques.[76] The experiment is based on sweeping the potential linearly with time and recording the current vs. voltage. This allows to study the redox processes of the electrodes in detail, being the current proportional to the different kinetic parameters, like the diffusion coefficient and the charge transfer constant. In a typical setup, the cell is composed of a working electrode, focus of the experiment, a counter electrode, to control the current, and a reference electrode, which acts as voltage reference.

In this work, CV was used to determine the electrochemical signature of the mesoporous titania, always acting as working electrodes. In **Paper 1**, CV measurements were performed with a three electrode T-cell setup to which lithium foil was used as counter and reference electrode. The working electrode and the counter electrode were pressed together with a separator between them. The cell was filled to the brim with electrolyte before the reference electrode was inserted. The cell was carefully closed and sealed with Parafilm ® laboratory film and aluminum foil to prevent leakage and evaporation of the electrolyte out of the cell and oxygen/moisture from entering the cell. The CV measurements were carried out at voltages from 0.7, 1.0, 1.3, or 1.7 to 2.9 V, respectively, in a Bio-Logic VMP-3 potentiostat. In **Paper 2**, CV measurements were performed on the half Li-ion cell in a Bio-Logic VMP-3 potentiostat at different scan rates. Moreover, CV measurements were performed on a three electrode T-cell setup to which silver foil was used as reference electrode and Kuraray YP 50F activated carbon as counter electrode. The CV measurements were carried out in a Bio-Logic VMP-3 potentiostat at different scan rates. Figure 5 reports the current vs voltage curves typical for the different types of electrochemical mechanisms presented in the thesis: capacitive, pseudocapacitive and faradaic.

4.2.2 Galvanostatic charge discharge (GCD)

Galvanostatic charge discharge (GCD), also called galvanostatic charging with potential limitation (GCPL) is a constant current based technique used to measure the variation of the potential with time.[76] This technique is useful to gain basic information on the electrochemical processes of the material under study, but it is also very suited to evaluate the cycling stability of single electrodes and devices. In **Paper I**, Galvanostatic charge discharge tests were performed between 0.7 V to 2.9 V in a Scribner 580 battery cycler. In **Paper 2**, Galvanostatic charge discharge tests were performed between 0 V to 2.9 V in a Scribner 580 battery cycler. Figure 6 reports the voltage vs. time curves for the different types of electrochemical mechanisms presented in the thesis: capacitive, pseudocapacitive and faradaic.

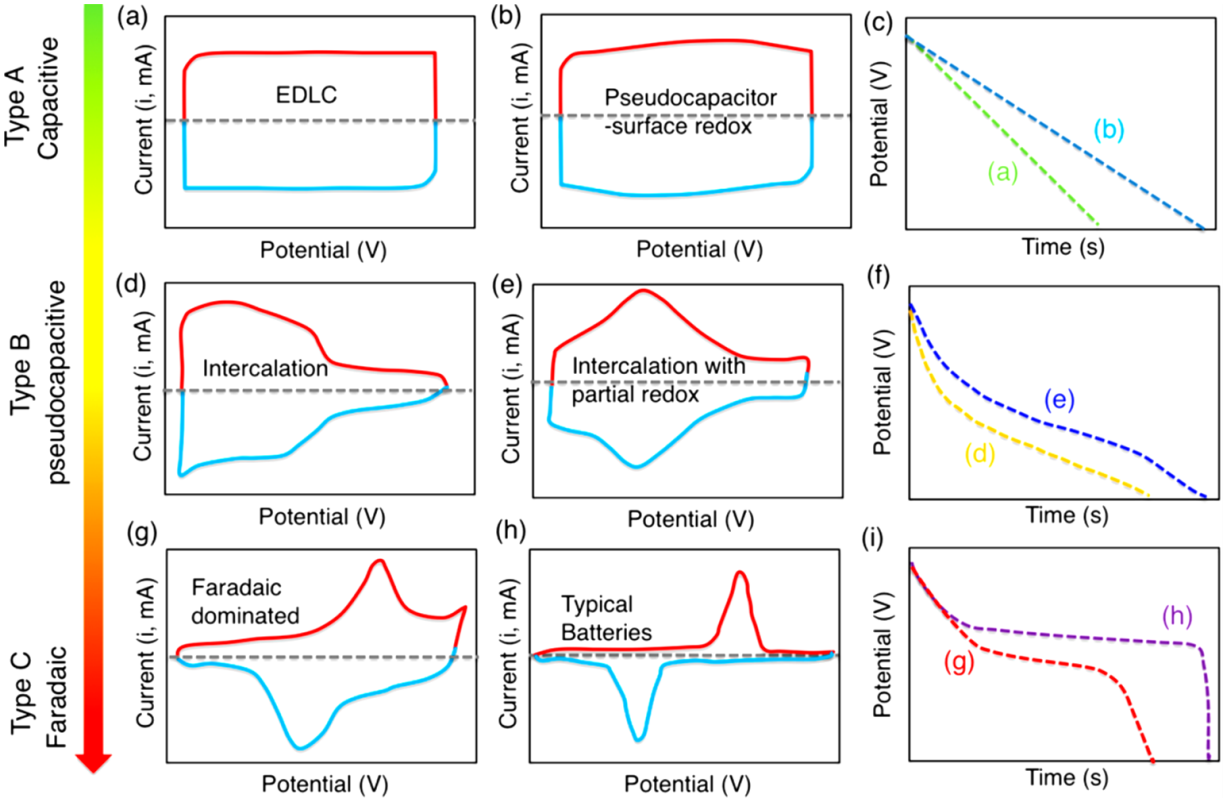

***Figure 6**: (a, b, d, e, g, h) Schematic cyclic voltammograms and (c, f, i) corresponding galvanostatic discharge curves for various kinds of energy-storage materials. A pseudocapacitive material will generally have the electrochemical characteristics of one, or a combination, of the following categories: (b) surface redox materials (d) intercalation-type materials, or (e) intercalation-type materials showing broad but electrochemically reversible redox peaks. Electrochemical responses in (g−i) correspond to battery-like materials. Reproduced with permission from (64)*

5. RESULTS AND DISCUSSION

5.1 Li-ion insertion mechanism in mesoporous titania

One of the main aims of this thesis is to present our understanding of the processes of Li^+ storage into the mesoporous titania materials. The first part of **Paper I** deals with the Li^+ ion insertion into the mesoporous anatase beads, while **Paper II** is focused on the lithiation of the ordered mesoporous amorphous titania. Both the evaluations were conducted in a half cell configuration with Li^+ as counter electrode, because in this configuration, the Li counter electrodes act as an infinite reservoir of Li^+ ions, allowing for a more accurate and focused study of the titania electrodes. The two materials store electrochemical energy storage through Li^+ ion insertion and extraction, however the mechanisms are different and consequently also the associated electrochemical signatures. These differences arise due to the specific structural features of the two materials. Thereby, it is important to combine electrochemical and structural characterization to gain a better picture of the processes involved. In the next paragraphs, the electrochemical performance of the mesoporous anatase beads is first reported, followed by the characterization of the mesoporous amorphous titania.

5.1.1 Mesoporous anatase titania beads

The TiO_2 beads crystal structure, morphology and mesoporosity were studied through XRD, N_2 adsorption and SEM, which is shown in Figure 7. The material is highly crystalline, showing only the anatase polymorphs and ~25 nm crystallites. The material consists of hierarchically organized micrometer sized beads with the mesopore dimension distributed around ~15 nm and a BET specific surface area of ~90 m^2/g.

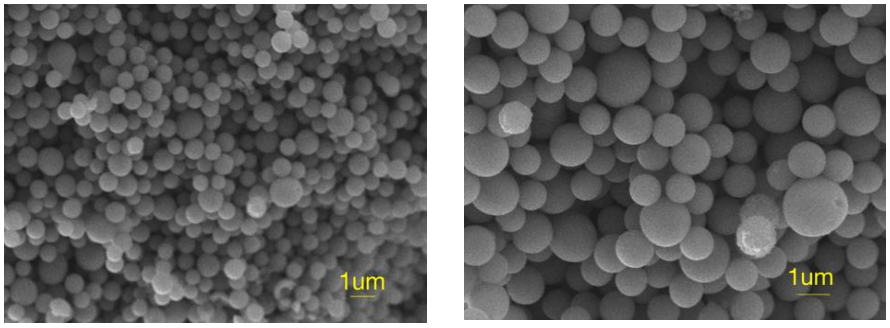

***Figure 7**: SEM micrographs of the TiO_2 beads in two magnifications. The 2nd panel clearly shows the aggregation of the nanoparticles in a spherical minimized surface energy structure.*

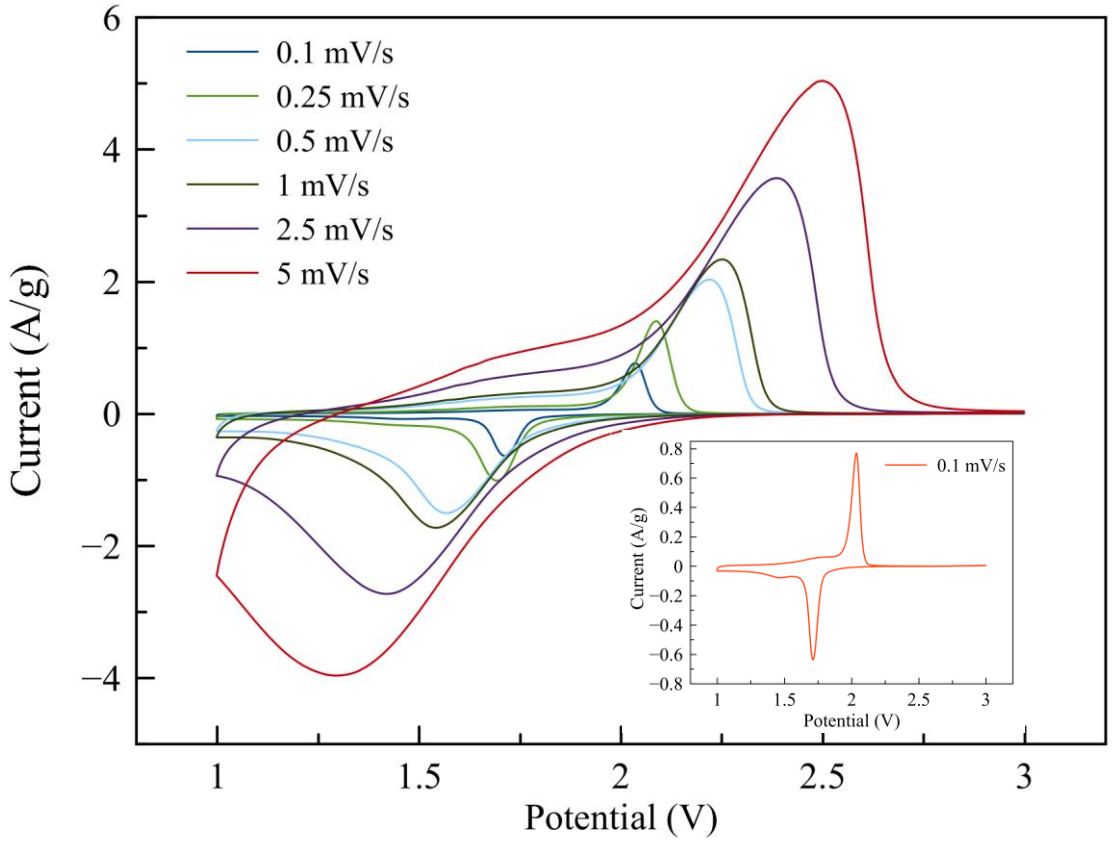

***Figure 8**: Cyclic voltammetry curves of the anatase beads vs. Li at the different scan rates of 0.1, 0.25, 0.5, 1, 2.5 and 5 mV/s. The inset reports a curve at 0.1 mV/s.*

Figure 8 reports the CV curves at scan rates from 0.1 to 5 mV/s, which exhibits typical and well-defined peaks. The hierarchical mesoporous structure allows for a complex storage of charges. Because of the specific surface area and the nanosized crystallites, three storage mechanisms can simultaneously take place: the formation of a double layer of charges associated to a capacitance, the redox Li insertion process, limited by diffusion, and fast surface redox processes giving rise to a pseudocapacitance of insertion type.[77] To differentiate between the different contributions to the total charge storage, the data from the CV curves performed at different rates are used. The relation between the measured current i and the scan rate ν provides an understanding of the mechanisms involved.

Following the treatment presented in **Paper I**, the relative capacitive contribution at the scan rate of 0.5 mV/s was calculated to be 30% of the total charge storage, as can be seen in Figure 9. At the scan rate of 5 mV/s the capacitive current is more significant and contributes for almost 60% of the total charge due to the rapid cycling. The double layer capacitance, which is proportional to the relatively low specific surface area, contributes little to the total capacitive contribution.

It follows that most of the capacitive current is pseudocapacitive in nature. This result further proves that the hierarchical structure allows for the mesoporous beads to be easily accessed by the electrolyte and undergo fast surface redox reactions.

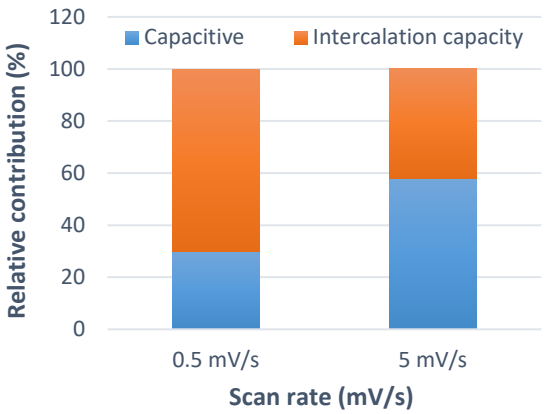

***Figure 9**: Relative contribution of the pseudocapacitive charge storage at 0.5 and 5 mV/s for the mesoporous anatase beads electrode.*

To further evaluate the cycling stability of the electrodes, GCD measurements were performed at the rate of 0.5C, which corresponds to 165 mAh g^{-1}. Figure 10 shows the GCD curves at different cycles and the discharge capacity vs. number of cycles. The potential vs capacity curves in panel (a) show three different regions and extended voltage plateaus corresponding to the anodic and cathodic peaks of the CV curves. The material is affected by irreversible capacity only for the first few cycles, showing stable performance afterwards with more than 95% capacity retention after 150 cycles. The mesoporous bead morphology demonstrates insertion/extraction reversibly for high amounts of lithium in applicable operating conditions.

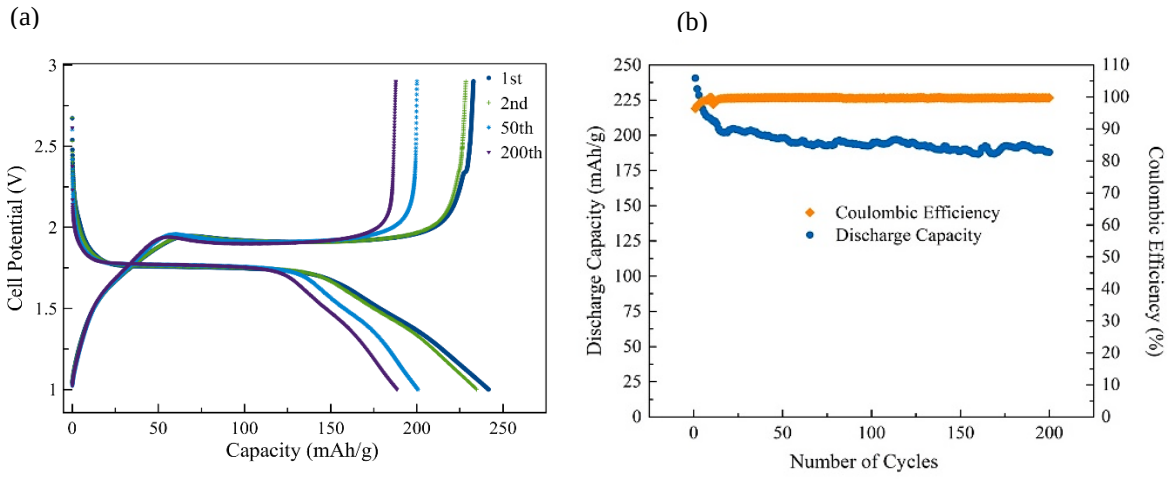

***Figure 10**: (a) GCD curves for the 1st, 2nd, 50th and 200th cycles at 0.5C. (b) discharge capacity and columbic efficiency vs. number of cycles*

Figure 11 reports the discharge capacities vs. number of cycles at different C rates of mesoporous anatase bead electrodes. The electrodes show very good rate performance, delivering 100 mAh g^{-1} at 10C, which means it is possible to charge the electrode in only 6 minutes, corresponding to 50% of the capacity storable in 2 hours. This remarkable high rate storage is possible thanks to the high pseudocapacitance shown by the material. Moreover, the high rate cycling is not damaging the mesoporous beads and, therefore, has a limited effect on the electrochemical performance. When the cycling rate step is reversed, the electrodes store a similar capacity when cycled at low rates. Figure 11 shows SEM images of a titania bead anode both in the pre-cycling and post-cycling conditions. The morphology of the beads in the post fast cycling condition looks practically identical to the pristine state. This result further proves the optimal stability of the mesoporous anatase beads morphology.

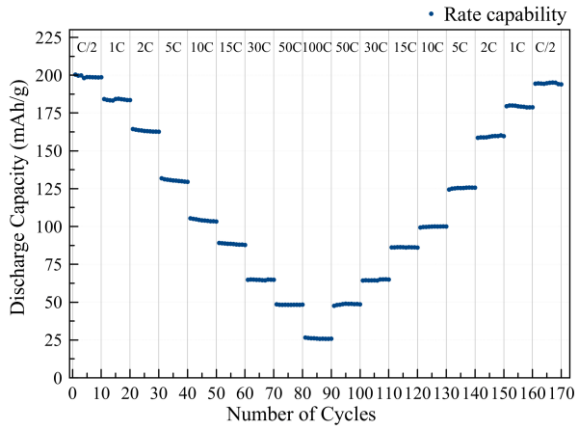

***Figure 11**: Rate performance for a mesoporous anatase beads electrodes.*

(a) (b)

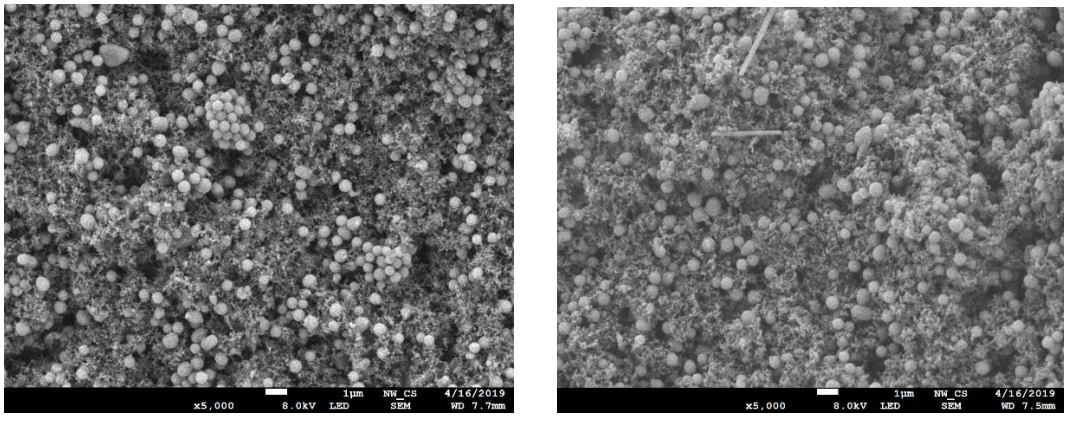

***Figure 12**: a) Pre-cycling TiO_2 electrode surface, b) post-cycling TiO_2 electrode surface.*

5.1.2 Mesoporous amorphous titania

In **Paper II**, Mesoporous amorphous titania structure was characterized with X-ray absorption spectroscopy (XAS), by studying the local environment of the titanium atom. To better understand its special features, Figure 13 reports also the spectrum of an anatase reference. In the theory of XAS the edge position is associated to the oxidation state of the element, which appears to be very similar in the two titania polymorphs (Ti^{4+}). The pre-edge region gives important information about the coordination and symmetry of the element. By studying the A1, A2 and A3 peaks position and intensity, it was be concluded that the mesoporous amorphous titania contains a combination of $^{[5]}$Ti and $^{[6]}$Ti, similarly to the findings of previous studies.[78,79,80] Amorphous titania nanoparticles seems to be composed of an anatase-like core with defects near the surface of the particle. Furthermore, the absence of a shoulder in the absorption edge of the mesoporous titania, further depicts a difference in symmetry of the titanium atom with the anatase material.

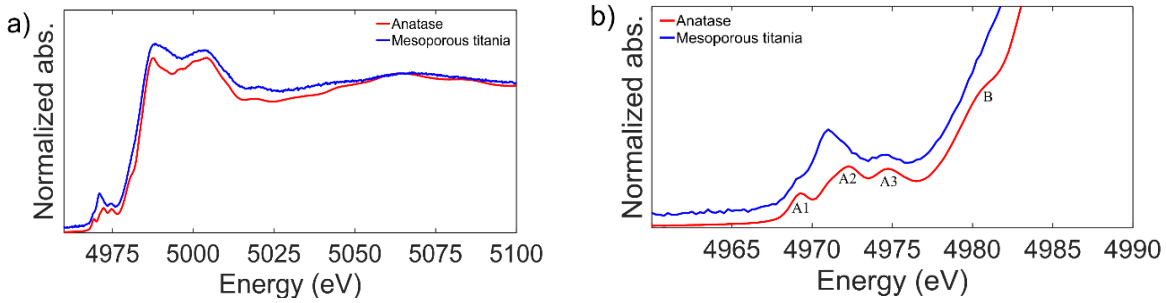

Figure 13: *XAFS spectra of the anatase and the pristine mesoporous titania samples. The pre-edge features are highlighted (b). The absorption spectra are shifted in intensity for clarity.*

The mesoporous amorphous titania electrodes were electrochemical characterized in a half cell configuration and the GCD curves between 2.9 V and 0.7 V are shown in Figure 14. The lower voltage limit was fixed to 0.7 V and not 1 V as in the anatase electrode because interesting electrochemical phenomena are taking place in the region between 1 V and 0.7 V. The mesoporous amorphous titania exhibits a quasi linear dependence of the stored charge with the potential through the charge/discharge curve. A very high capacity of ~680 mAh g^{-1} is observed for the first discharge cycle, and then the capacity decreases rapidly in the subsequent cycles, with the second cycle retaining only 40% of the initial capacity (~280 mAh g^{-1}). Figure 12b reports CV tests at the scan rate of 0.3 mV/s. The mesoporous amorphous titania shows a pseudocapacitive behavior of insertion type, extrinsically due to the mesoporous morphology and intrinsically due to the amorphous structure. The apparently under-coordinated Ti atom in the mesoporous material may explain its intrinsic pseudocapacitance.

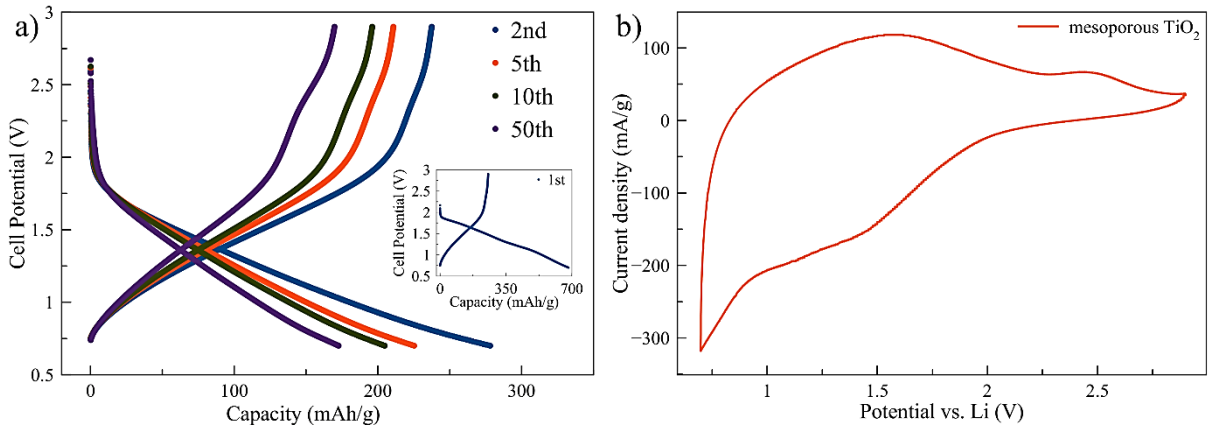

Figure 14. *a) Charge/discharge curves of mesoporous titania electrodes between 2.9 V and 0.7 V cycled at 0.5 C. b) cyclic voltammetry curves (10th cycle) scanned between 2.9 V and 0.7 V for mesoporous titania at the scan rate of 0.3 mV/s.*

Figure 15 presents further electrochemical characterization of the mesoporous amorphous titania. The initial large irreversibility is concentrated during the first 20 cycles. The capacity fading after the 20th cycle is slower and the electrode shows 80% capacity retention for almost 200 cycles, as shown in Figure 13a. The Figure 13b presents a good rate capability, with 83 mAh g^{-1} delivered at 10 C and high recovery of capacity when cycling the electrode again at lower rates.

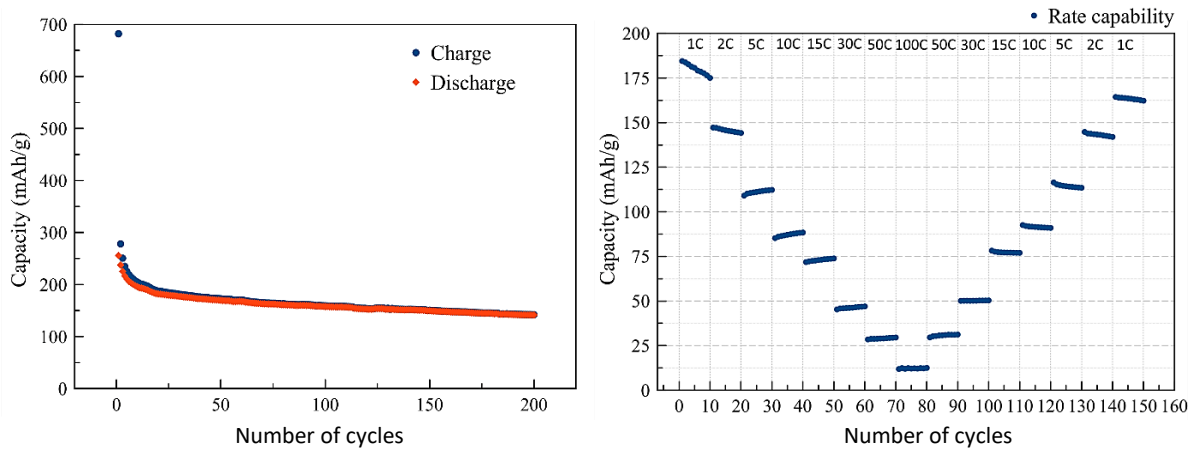

Figure 15. *Charge and discharge capacity vs. number of cycles (a) and the performance at higher rates (b) of the mesoporous titania electrodes.*

The 10 C capacity value is smaller compared to the one shown by the mesoporous anatase beads (100 mAh g^{-1}). However, the mesoporous amorphous titania could in theory perform better at high rates thanks to its pseudocapacitive behaviour of both extrinsic and intrinsic character. We believe that the large irreversibility exhibited in the first cycles might be the reason for this lack in performance. Therefore, a combination of CV, XAS and TEM have been used to study the origin of the irreversibility and the associated structural changes in the material.

5.1.3 Origin of the irreversibility in the mesoporous amorphous titania

CV tests with cut-off voltages of 1.7, 1.3, 1.0 and 0.7 V were performed and are shown for electrodes cycled for 50 cycles in Figure 16.

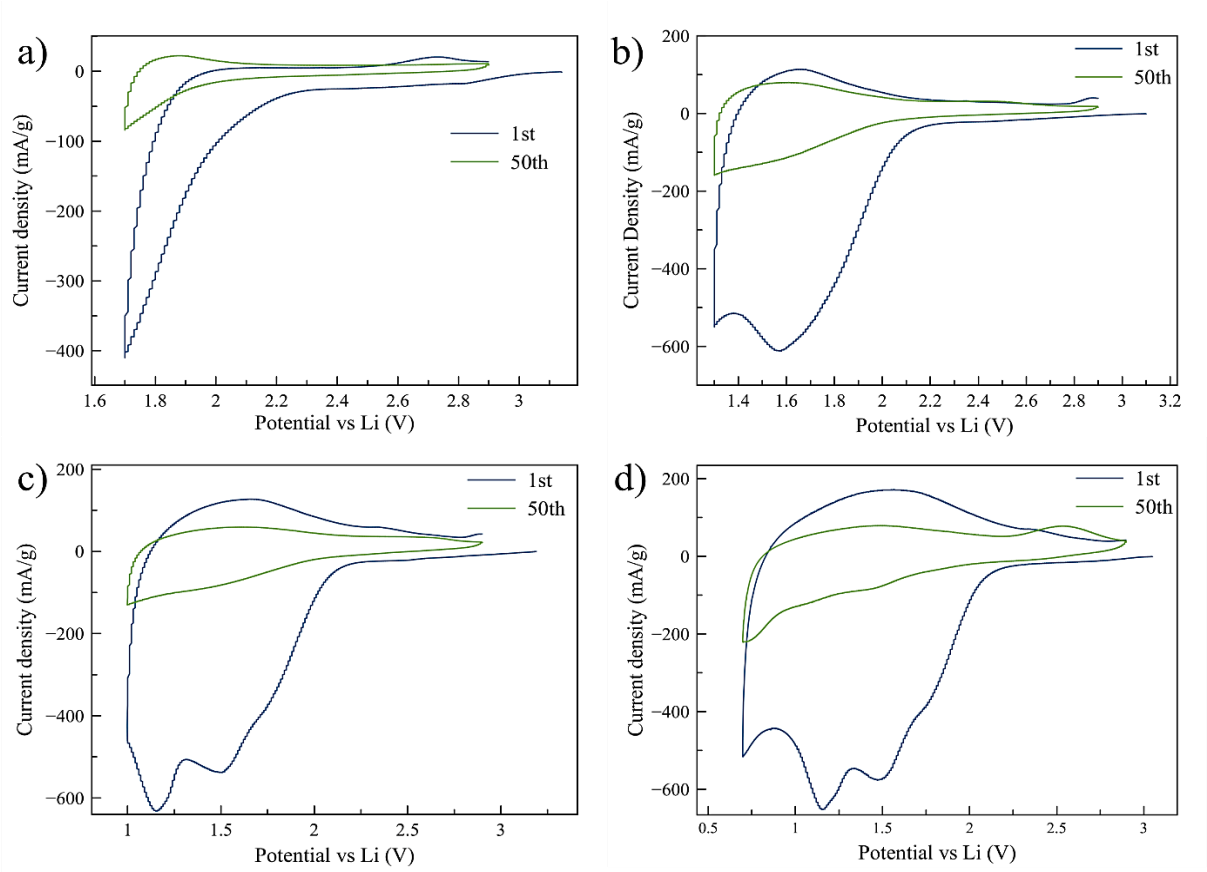

Figure 16. *Cyclic voltammetry scans performed with a three-electrode setup at 0.3 mV/sec between 2.9 V and 1.7 V (a), 2.9 and 1.3 V (b), 2.9 and 1.0 V (c), and 2.9 and 0.7 V (d). The first and fiftieth cycle of each CV are shown in the graphs.*

A large irreversibility is observed already at 1.7 V, even though the concentration of Li ions inserted in the titania structure is typically low with $x < 0.5$ in Li_xTiO_2. Figure 16d shows the presence of four different reduction peaks, which we believe are associated to the formation of stable and electrochemically inactive phases. The peak at 0.7 V is believed to be originated from the formation of a solid electrolyte interface (SEI). To investigate the structural changes associated to the other peaks, XAS and TEM were used.

XAS measurements were performed on the previously cycled samples, in both the intercalated (0.7 V) and deintercalated (2.9 V) states, as reported in Figure 17.

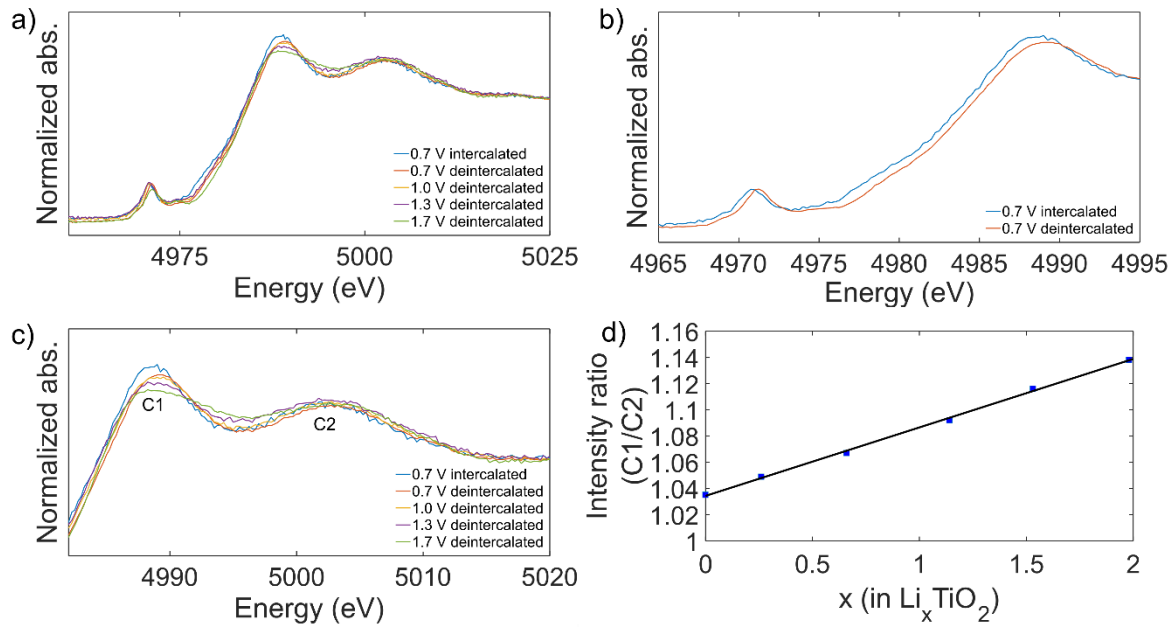

Figure 17*. XAS spectra of the cycled samples (a) and a comparison of the intercalated and the deintercalated state of the samples cycled to 0.7 V, showing a shift in the edge position (b). The post-edge region of the XAS spectra of pristine and cycled mesoporous titania is highlighted (c) and the effect of the lithium concentration on the peak intensity ratio C1/C2 (d). The point at x=0 is for the pristine sample.*

The post-edge or NEXAFS region, containing spectral features associated to multiple scattering phenomena, gives some interesting information on the structural changes during the lithiation process.[81,82,83] In Figure 17c it is observed that the peak intensity C1/C2 increases with lower cutoff potential and at cut-off potential 0.7 V, the sample in the intercalated state has a higher peak ratio than the sample in the deintercalated state. It appears that the presence of irreversibly bound lithium affects the multiple scattering processes. The concentration of irreversibly bound lithium conceivably increases with lower cut-off potential and consequently has a larger impact on the MS processes, as seen in the shift in the ratio of the intensity of the C1/C2 peaks in Figure 17d. From the graph it is observed that there is a linear correlation between the lithium concentration and the intensity ratio of peak C1 to C2. This linear relationship is valid for electrodes in the deintercalated state and in the intercalated state, containing also reversibly bound lithium. This shows that the local environment of the titanium atom is affected in a similar way by the different lithium intercalation phenomena occurring during cycling, further indicating that the distance between the inserted lithium atoms and the titanium atom is very similar regardless if the lithium is reversibly or irreversibly bound. Because of this indistinguishable effect on the multiple scattering, we conclude

that lithium is always positioned in the close proximity of the titanium atom forming Li_xTiO_2 species. This also implies that formation of lithium containing species outside the near environment of the titania structure, such as lithium oxide, is improbable in our system.

TEM imaging was then used to verify the formation of Li_xTiO_2 species. In a previous publication, it was shown that the titania material is mesoporous and contains small anatase crystallites.[72] Bright field (BF) and high resolution (HR) TEM images of the electrode, composed of mesoporous titania in a carbon matrix, cycled to 1.7 V and interrupted in the deintercalated state, are shown in Figure 18a-d. The image in panel d shows a crystal of ~15nm, which was found to correspond to the {400} planes of $LiTiO_2$. The crystalline lithium titanate formation can be associated to the reduction peak at 1.7 V, seen in the CV measurements (Figure 18a). Interestingly, it appears that the formation of lithium titanate is caused by local crystallization phenomena at average Li concentration below x = 1 in Li_xTiO_2, and partly responsible for the irreversible capacity.

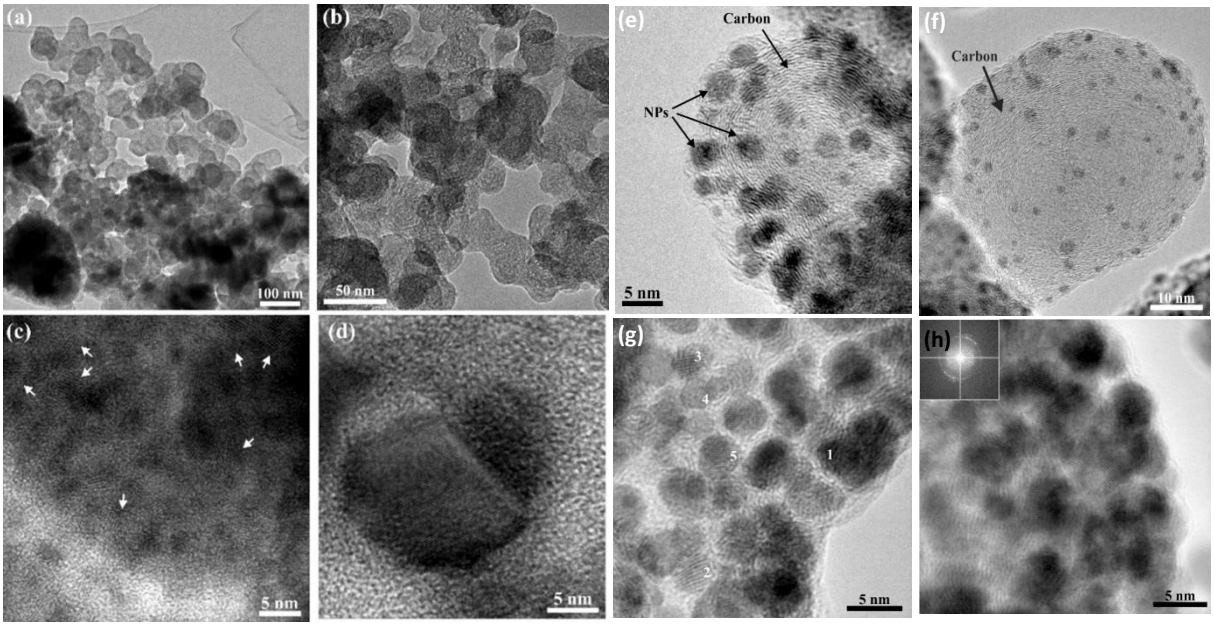

Figure 18. *Bright field TEM images of the electrode cycled to 1.7 V showing the overall morphology of the sample (a, b) and HR-TEM images showing the nanocrystalline anatase (c) and LiTiO2 (d). BFTEM images of the electrode cycled to 1.0 V which consist of carbon particles incorporating smaller crystalline nanoparticles (e, f). HRTEM images used for d-spacing measurements (g). The inset shows the FFT diffractogram that corresponds to the whole image (h).*

Figure 18e-h shows TEM images of the electrode cycled to 1.0 V and interrupted in the de-intercalated state. To establish the nature of the crystalline nanoparticles, the d-spacing was determined with a combination of analysis of the lattice fringes and measurements based on the reflections present in the FFT from the nanoparticle area. The phases investigated as possible structures are anatase, lithium oxide (Li_2O) and lithium titanate ($LiTiO_2$). The observed linearity between the shift of the C1/C2 intensity ratio and the lithium concentration (Figure 17d) supports the hypothesis that more $LixTiO_2$ phases were formed in the electrode. It should be stated that the mesoporous titania material contains a large amount of amorphous phase, which is not readily detected in the TEM images, and the associated lithium containing phases are, presumably, partly amorphous as well.

To further examine the electrode, including the amorphous phases, and to get more insight on the irreversibly bound lithium distribution, energy filtered (EF) TEM experiments were performed on the electrode cycled to 1.0 V and interrupted in the deintercalated state. The areas were energy filtered so that the maps of Li, Ti and O elemental distributions were obtained. As can be seen in Figure 19, Li appears to be located mainly at the surface while Ti and O are distributed over the whole area. Considering the nature of the amorphous titania phase, which contains a large number of defects near the surface, and the lithium-titanium elemental map, it appears that the irreversible phases are mainly located at the surfaces. The high quantity of lithium observed in the energy filtered images is in line with the large irreversibility observed in the CV curve of the electrode. Furthermore, the composite elemental maps show that lithium is located in close proximity with both titanium and oxygen, which is in line with our hypothesis that irreversible Li_xTiO_2 species are formed during the cycling of the electrodes.

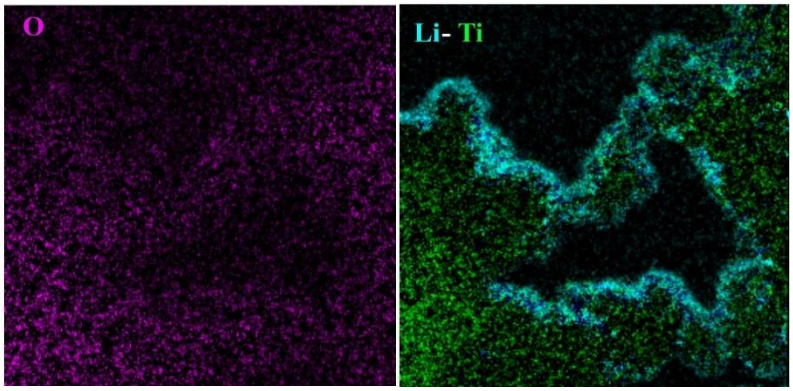

Figure 19*: Unfiltered (BF), energy filtered images, and composite elemental maps of the mesoporous titania cycled to 1.0 V. From the composite elemental maps, it can be seen that Li appears to be located mainly at the surface while Ti, and O are distributed over the whole area.*

The formation of irreversibility on the surface of the material can be also the reason for the lower rate capability of the mesoporous amorphous titania compared to the mesoporous anatase beads. We believe that the irreversible phases possibly reduce the diffusion rate of Li ions inside the titania structure. Further study needs to be done to verify this conclusion.

5.2 Mesoporous TiO_2 beads as negative electrode for asymmetric supercapacitor

From the results reported in the previous section, the mesoporous anatase beads seems to be a perfect candidate as a negative electrode in a hybrid asymmetric supercapacitor. Commercial activated carbon was used as material for the positive electrode. As reported before, the anatase titania electrode stores energy through Li^+ ions intercalation into its structure. Whereas, the porous activated carbon stores charges through the adsorption of anions on its very high surface (~1.800 m^2/g), forming a double layer of charges.[84] The formation of the double layer is associate to a linear plot of the voltage vs. time. To achieve charge balance, the positive electrode must have a mass 8 times bigger than the negative electrode. To distinguish and appreciate the contributions of the single electrodes to the overall cell voltage, a three-electrode cell was built with Ag as reference electrode. A GCD measurement conducted at 2.5 A g^{-1} and reporting the waveform for the cell, the titania and the carbon is presented in Figure 20.

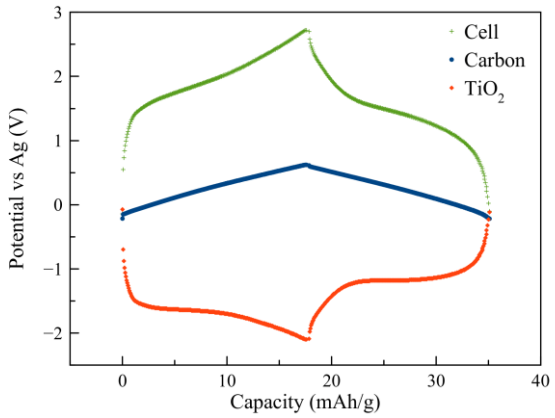

***Figure 20**: Galvanostatic charge/discharge curve at 2.5 A g^{-1} vs. Ag, for an asymmetric supercapacitor.*

The long-term cycling ability of the device is shown in Figure 21. In panel a, we can see an initial decrease in capacity for the first 50 cycles, which can be associated to the initial irreversibility of the anatase beads. This irreversibility does not affect the remarkable stability of the device that shows 93% of capacity retention over 10000 cycles. Furthermore, as reported in panel b, the average specific energy of ~27 mWh g^{-1} is maintained stable along the 10000 cycles.

To our knowledge this is one of the best performances ever reported in literature for hybrid asymmetric supercapacitors.[10,85,86,87]

The energy efficiency is also improving during the first 500 cycles and gradually stabilizing to 80%, which means that continued cycling is not damaging the material by inducing a strain overpotential.

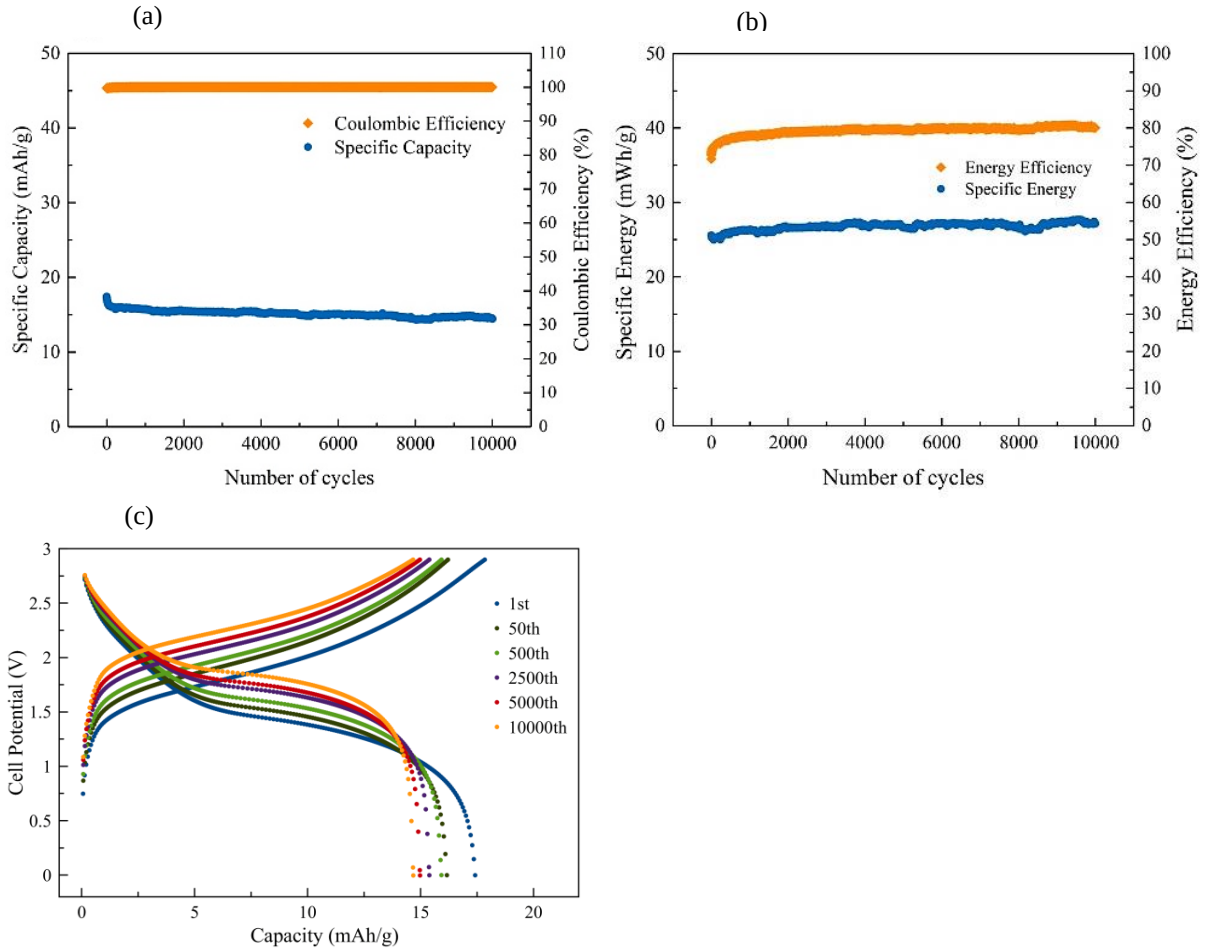

Figure 21: *Hybrid asymmetric supercapacitor´s GCD performance: (a) capacity and columbic efficiency vs. number of cycles; (b) energy and energy efficiency vs. number of cycles; (c) GCD potential vs. capacity reported for the 1st, 50th, 500th, 2500th, 5000th, 10000th cycles.*

The high energy stability is connected to a gradual shift of the potential along the cycling as shown in Figure 21c. More interestingly, a balancing effect is taking place, where the progressive reduction of the capacity, due to a reasonable electrode degradation, is balanced by the translation of both cathodic and anodic plateaus to higher values.

A further analysis with GCD in the three-electrode configuration mentioned before, reveals that both the electrodes have a change in their overpotential during the cycling, as can be seen in Figure 22 for the full cell charging process. Further combination of electrochemical and structural characterization will be necessary to understand this curious phenomenon.

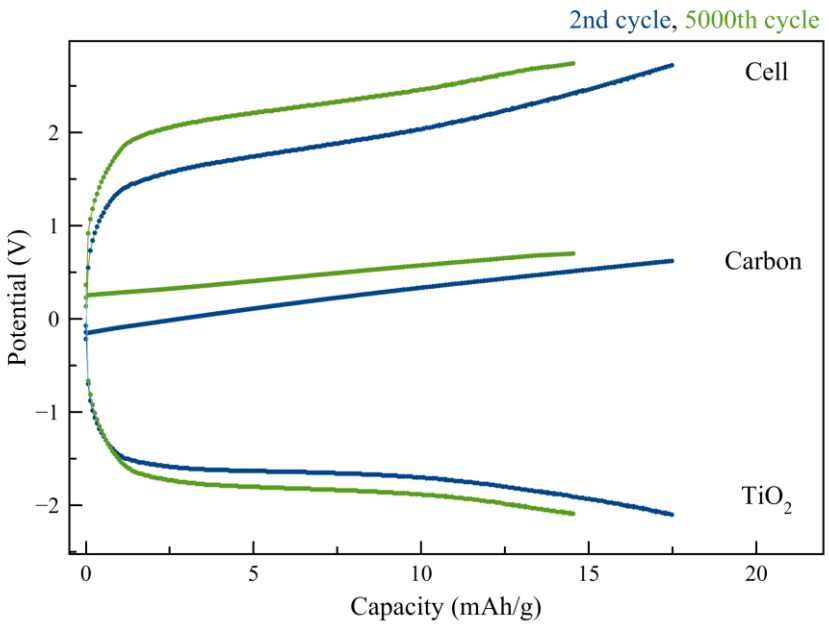

***Figure 22**: GCD measurement at 2.5 Ag^{-1} showing the overpotential shift of the electrodes and the total cell, during charging of the device.*

The cycling at different rates and the energy density *vs* the power density performance (Ragone Plot) are shown in Figure 23. The plot reports the gravimetric densities, measured with respect to the total mass of the electrodes, and the volumetric energy density, also considering the electrolyte and the separator. Our supercapacitor delivers 37 Wh kg^{-1} at 0.5A g^{-1} (100 W kg^{-1}) and it is still providing ~10 Wh kg^{-1} at the very high current of 20A g^{-1} (3kW kg^{-1}).

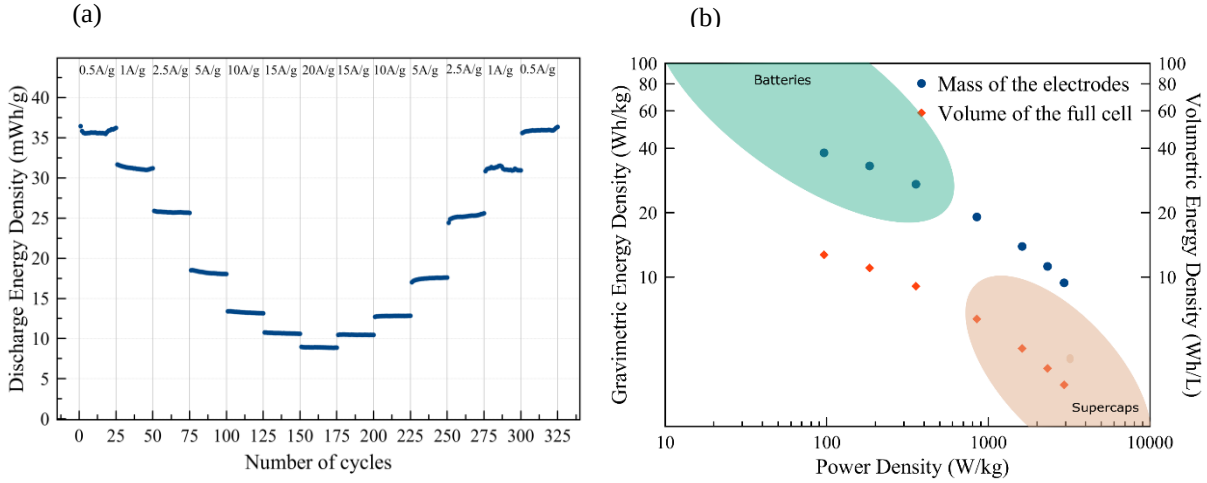

***Figure 23**: (a) Rate performance of the asymmetric supercapacitor and (b) Ragone plot reported in terms of mass of the electrodes or volume of the full cell.*

6. CONCLUSION AND FUTURE WORK

The lithiation of ordered mesoporous titania and mesoporous anatase bead electrodes was characterized and compared. We conclude that the difference in the polymorphs structure has a pronounced effect on the electrochemical mechanisms and performance of the two materials.

The ordered mesoporous titania has a very high initial electrochemical capacity of 680 mAh g^{-1} in the first cycle, but the capacity quickly fades and is ~170 mAh g^{-1} after 50 cycles. The mesoporous titania performed well in the rate capability test, delivering 83 mAh g^{-1} at 10C. The large irreversibility of the material was analyzed by cyclic voltammetry and structural characterization was performed by TEM and XAS. The CV revealed that the irreversibility occurs already at 1.7 V, at the position of the first peak which was found to be associated with the formation of crystalline lithium titanate ($LiTiO_2$). XAS measurements showed that irreversibly and reversibly intercalated lithium affect the multiple scattering in the NEXAFS region. By comparing peak intensity ratios in the NEXAFS region, we propose a method to differentiate between lithium bound in close proximity and lithium located further away from the titanium atom. The mesoporous titania shows many similarities to amorphous titania, which contains high amounts of defects near the surface. We suggest that the presence of such defects leads to the formation of irreversible phases mainly located at the surface of the material. The effect of these irreversible phases on the rate performance of the material needs to be further study.

The mesoporous anatase bead electrodes showed the typical Li ion intercalation signature. However, calculations reveal that a large contribution to the stored charge is of extrinsic pseudocapacitive nature. The electrodes show high specific capacities of 200 mAh g-1, with more than 90% capacity retention over 200 cycles and very good rate capabilities, retaining 100 mAh g^{-1} at 10C rate. The mesoporous bead electrode was therefore used as negative electrode in a hybrid asymmetric supercapacitor, with commercial activated carbon as positive electrode. The device delivers 37 Wh kg^{-1} at 0.5 A g^{-1} (100 W kg^{-1}) and almost 10 Wh kg^{-1} at the very high current of 20 A g^{-1} (3 kW kg^{-1}). The device showed very stable performance, with no decrease in specific energy over 10000 cycles, involving a curious gradual shift to higher potentials counter balancing a gradual decrease in capacity.

Further combination of electrochemical and structural characterization will be necessary to understand this curious phenomenon. Moreover, to improve the rate performance of the mesoporous anatase bead material, we are currently studying the effect of niobium doping. The high stability of the system and the use of low cost and environmentally friendly materials are paving the way to a possibly marketable system.

7. ACKNOWLEDGEMENTS

I would like to acknowledge the Swedish Energy Agency (Energimyndigheten) for funding.

Thanks to my supervisor Anders Palmqvist, for giving me the opportunity to start my PhD path. Thanks for always being open minded about my ideas and for the fruitful discussions. Your tendency towards improvement, being it regarding research or our University, really inspires me. Tack för alla möjligheterna du gav mig under dessa år.

Thanks to my examiner Magnus Skoglundh for the very useful advices and the positivity you radiate. Thanks to my previous studierektor, Hanna Härelind, and current one, Lars Nordstierna. It is always pleasant and enriching to communicate with you.

Thanks to my co-supervisor Aleksandar Matic, for making me feel part of the KMF family. Thanks for all the opportunities and advices. Thanks to all the KMF group and its the previous members. You are a great combination of brightness and fun.

I couldn´t expect a more diverse, interesting and funny environment then the one of the Diamond Division. Thanks to all of you for this amazing time, to be cool colleagues and good friends. Thanks to my group, you really are a precious gift.

Gunnar, it was a great experience to write a paper with you! Thanks for the support and for the patience.

A special acknowledgment goes to Dr. Carmen Cavallo. Grazie per essere stata sempre presente, per il continuo supporto, per non mollare mai. Sei una forza e una vera amica!

Finally, thanks to all my friends and my family for everything. Thanks Andrea for being by my side :)

8. REFERENCES

1. "Key World Energy Statistics 2018", https://www.iea.org/
2. Chu, S. & Majumdar, A. Opportunities and challenges for a sustainable energy future. *Nature* 488, 294–303 (2012).
3. Elmqvist, T., Andersson, E., Frantzeskaki, N., McPhearson, T., Olsson, P., Gaffney, O., Takeuchi, K. & Folke, C. Sustainability and resilience for transformation in the urban century. *Nat. Sustain.* 2, 267 (2019).
4. Armand, M. & Tarascon, J.-M. Building better batteries. *Nature* 451, 652–657 (2008).
5. Larcher, D. & Tarascon, J.-M. Towards greener and more sustainable batteries for electrical energy storage. *Nature Chem.* 7, 19–29 (2015).
6. Liu, Y. & Yang, Y. Recent Progress of TiO2-Based Anodes for Li Ion Batteries. *J. Nanomat.* (2016). doi:10.1155/2016/8123652
7. Tarascon, J.-M. & Armand, M. Issues and challenges facing rechargeable lithium batteries. *Nature* 414, 359 (2001).
8. Winter, M. & Brodd, R. J. What Are Batteries, Fuel Cells, and Supercapacitors? *Chem. Rev.* 104, 4245–4270 (2004).
9. Simon, P., Gogotsi, Y. & Dunn, B. Where Do Batteries End and Supercapacitors Begin? *Science* 343, 1210–1211 (2014).
10. Shao, Y., El-Kady, F. M., Sun, J., Li, Y., Zhang, Q., Zhu, M., Wang, H., Dunn, B. & Kaner, R. B. Design and Mechanisms of Asymmetric Supercapacitors. *Chem. Rev.* 118, 9233–9280 (2018).
11. Chen, G. Z. Supercapacitor and supercapattery as emerging electrochemical energy stores. *Int. Mater. Rev.* 62, 173–202 (2017).
12. Gogotsi, Y. What Nano Can Do for Energy Storage. *ACS Nano* 8, 5369–5371 (2014).
13. Rolison, D., R., Long, J. W., Lytle, J. C., Fischer, A. E., Rhodes, C. P., McEvoy, T. M., Bourg, M. E. & Lubers, A. M. Multifunctional 3D nanoarchitectures for energy storage and conversion. *Chem. Soc. Rev.* 38, 226–252 (2008).
14. Brousse, T., Bélanger, D. & Long, J. W. To Be or Not To Be Pseudocapacitive? *J. Electrochem. Soc.* 162, A5185–A5189 (2015).
15. Augustyn, V., Come, J., Lowe, M. A., Kim, J., W., Taberna, P.-L., Tolbert, S. H., Abruna, H. D., Simon, P. & Dunn, B. High-rate electrochemical energy storage through Li^+ intercalation pseudocapacitance. *Nat. Mater.* 12, 518–522 (2013).
16. Augustyn, V., Simon, P. & Dunn, B. Pseudocapacitive oxide materials for high-rate electrochemical energy storage. *Energy Environ. Sci.* 7, 1597–1614 (2014).

17. Borghols, W. J. H., Lützenkirchen-Hecht, D., Haake, U.; Chan, W., Lafont, U., Kelder, E. M., van Eck, E. R. H., Kentgens, A. P. M., Mulder, F. M., Wagemaker, M. Lithium Storage in Amorphous TiO2 Nanoparticles. *J. Electrochem. Soc.* 157, 582–588 (2010)
18. Ryu, W. H., Nam, D. H., Ko, Y. S., Kim, R. H., Kwon, H. S. Electrochemical Performance of a Smooth and Highly Ordered TiO2 Nanotube Electrode for Li-Ion Batteries. *Electrochim. Acta* 61, 19–24 (2012)
19. Moitzheim, S., De Gendt, S., Vereecken, P. M. Investigation of the Li-Ion Insertion Mechanism for Amorphous and Anatase TiO2 Thin-Films. *J. Electrochem. Soc*. 166, 1–9 (2019)
20. Encyclopedia of Electrochemical Power Sources | ScienceDirect. Available at: https://www.sciencedirect.com/referencework/9780444527455/encyclopedia-of-electrochemical-power-sources
21. Dell, R. M. Batteries: fifty years of materials development *Solid State Ion.*, 134, 139-158 (2000)
22. Whittingham, M. S. Electrical Energy Storage and Intercalation Chemistry. *Science* 192, 1126–1127 (1976).
23. Mizushima, K., Jones, P. C., Wiseman, P. J. & Goodenough, J. B. LixCoO2 *Materials Research Bulletin* 15, 783–789 (1980).
24. Yoshino A., Converting carbon material into a battery negative electrode, TANSO (Journal of The Carbon Society of Japan),186,45–49 (in Japanese) (1999)
25. Fong, R., von Sacken, U. & Dahn, J.R. Studies of Lithium Intercalation into Carbons Using Nonaqueous Electrochemical Cells. *J. Electrochem. Soc.* 137, 2009-2013 (1990)
26. Nitta, N., Wu, F., Lee, J. T., Yushin, G. Li-Ion Battery Materials : Present and Future. *Mater. Today* 18 , 252–264 (2015)
27. Liu, J., Kopold, P., vanAken, P. A., Maier, J., Yu, Y. Energy Storage Materials from Nature through Nanotechnology: A Sustainable Route from Reed Plants to a Silicon Anode for Lithium-Ion Batteries. *Angew. Chemie - Int. Ed.* 54, 9632–9636 (2015)
28. Zhang, W.-M.; Hu, J.-S.; Guo, Y.-G.; Zheng, S.-F.; Zhong, L.-S.; Song, W.-G.; Wan, L.-J. Tin-Nanoparticles Encapsulated in Elastic Hollow Carbon Spheres for High-Performance Anode Material in Lithium-Ion Batteries. *Adv. Mater.* 20, 1160–1165 (2008)
29. Zuo, X.; Zhu, J., Müller-Buschbaum, P., Cheng, Y. J. Silicon Based Lithium-Ion Battery Anodes: A Chronicle Perspective Review. Nano Energy 31, 113–143 (2017)
30. Battery requirements for future automotive applications, https://eucar.be/
31. Conway, B. E. Electrochemical Supercapacitors: Scientific Fundamentals and Technological Applications. Springer US (1999).

32. Simon, P. & Gogotsi, Y. Materials for electrochemical capacitors. *Nature Materials* 7, 845–854 (2008).
33. Stern, 0. Zur theorie der elektrolytischen doppelschicht. *Z. Elektrochem. Angew. Phys. Chem*. 30, 508-516 (1924)
34. Bolt, G. H. Analysis of the validity of the Gouy-Chapman theory of the electric double layer. *J. Colloid Sci.* 10, 206–218 (1955).
35. Grahame, D. C. Diffuse Double Layer Theory for Electrolytes of Unsymmetrical Valence Types. *J. Chem. Phys.* 21, 1054–1060 (1953).
36. Frackowiak, E. Carbon materials for supercapacitor application. *Phys. Chem. Chem. Phys.* 9, 1774–1785 (2007).
37. Zhong, C., Deng, Y., Hu, W., Qiao, J., Zhang, L., Zhang, J. A review of Electrolyte Materials and Compositions for Electrochemical Supercapacitors. *Chem. Soc. Rev.* 44, 7484−7539. (2015)
38. Chmiola, J., Yushin, G., Portet, C., Simon, P., Taberna, P.L. Anomalous increase in carbon capacitance at pore sizes less than 1 nanometer. *Science* 313, 1760–1763 (2006).
39. Trasatti, S., Buzzanca, G., Ruthenium dioxide: A new interesting electrode material. Solid state structure and electrochemical behaviour. *J. Electroanal. Chem. Interfacial Electrochem*. 29, 1-5 (1971)
40. Toupin, M., Brousse, T., Belanger, D., Charge Storage Mechanism of MnO_2 electrode used in aqueous electrochemical capacitor *Chem. Mater* 16, 3184-3190 (2004)
41. Sathiya, M., Prakash, A.S., Ramesha, K., Tarascon, J.M., Shukla, A.K., V_2O_5-anchored carbon nanotubes for enhanced electrochemical energy storage. *J. Am. Chem. Soc.* 133, 16291-16299 (2011)
42. Come, J., Augustyn, V., Kim, J.W., Rozier, P., Taberna, P.L., Gogotsi, P., Long, J.W., Dunn, B., Simon, P. Electrochemical kinetics of nanostructured Nb_2O_5 electrodes. *J. Electrochem. Soc.* 161, 718-725 (2014)
43. Ryu, K.S., Kim, K.M., Park, N.-G, Park, Y.J., Chang, S.H., Symmetric redox supercapacitors with conductive polyaniline electrodes. *J. Power Sources* 103, 305-309 (2002)
44. Laforgue, A., Simon, P., Sarrazin, C. & Fauvarque, J.-F. Polythiophene-based supercapacitors. *J. Power Sources* 80, 142–148 (1999).
45. Opitz, M., Yue, J., Wallauer, J., Smarsly, B. & Roling, B. Mechanisms of Charge Storage in Nanoparticulate TiO2 and Li4Ti5O12 Anodes: New Insights from Scan rate-dependent Cyclic Voltammetry. *Electrochim. Acta* 168, 125–132 (2015).
46. Okubo, M. et al. Nanosize Effect on High-Rate Li-Ion Intercalation in LiCoO2 Electrode.

J. Am. Chem. Soc. 129, 7444–7452 (2007).

47. Ruiz-Rosas, R. Design of hybrid asymmetric capacitors in aqueous electrolyte using ZTC and ultraporous activated carbons. Diseño de condensadores asimétricos híbridos en electrolito acuso mediante ZTC y carbones activados utraporosos. *Boletín del Grupo Español del Carbón* 2015, 37, 14.
48. Evanko, B., Boettcher, S. W., Yoo, S. J. & Stucky, G. D. Redox-Enhanced Electrochemical Capacitors: Status, Opportunity, and Best Practices for Performance Evaluation. *ACS Energy Lett.* 2, 2581–2590 (2017).
49. Khomenko, V., Raymundo-Piñero, E., Frackowiak, E. & Béguin, F. High-voltage Asymmetric Supercapacitors Operating in Aqueous Electrolyte. *Appl. Phys. A* 82, 567–573 (2006).
50. Betz, J., Bieker, G., Meister, P., Placke, T., Winter, M. & Schmuch, R. Theoretical versus Practical Energy: A Plea for More Transparency in the Energy Calculation of Different Rechargeable Battery Systems. *Adv. Energy Mater.* 9, 1803170 (2019).
51. Gogotsi, Y. & Simon, P. True Performance Metrics in Electrochemical Energy Storage. *Science* 334, 917–918 (2011).
52. Li, B., Zheng, J., Zhang, H., Jin, L., Yang, D., Lu, H., Shen, C., Shellikeri, A., Zheng, Y., Gong, R., Zheng, J. P. & Zhang, C. Electrode Materials, Electrolytes, and Challenges in Nonaqueous Lithium-Ion Capacitors. *Adv. Mater.* 30, 1705670-1705690 (2018)
53. Ding, J., Hu, W., Paek, E. & Mitlin, D. Review of Hybrid Ion Capacitors: From Aqueous to Lithium to Sodium. *Chem. Rev.* 118, 6457–6498 (2018).
54. Amatucci, G.G., Badway, F., Du Pasquier, A., Zheng, T., An Asymmetric Hybrid Nonaqueous Energy Storage Cell. *J. Electrochem. Soc.* 148, 930-939, (2001)
55. Berger, T., Monllor-Satoca, D., Jankulovska, M., Lana-Villarreal, T. & Gómez, R. The Electrochemistry of Nanostructured Titanium Dioxide Electrodes. *Chem.Phys.Chem* 13, 2824–2875 (2012).
56. Chen, X. & Mao, S. S. Titanium Dioxide Nanomaterials: Synthesis, Properties, Modifications, and Applications. *Chem. Rev.* 107, 2891–2959 (2007).
57. Zhang, H., Chen, B., Banfield, J. F., Waychunas, G. A. Atomic Structure of Nanometer-Sized Amorphous TiO_2. *Phys. Rev. B - Condens. Matter Mater. Phys.* 78, 1–12 (2008)
58. Mi, J. L., Jensen, K. M. Ø., Tyrsted, C., Bremholm, M., Iversen, B. B. In Situ Total X-Ray Scattering Study of the Formation Mechanism and Structural Defects in Anatase TiO_2 Nanoparticles under Hydrothermal Conditions. *Cryst.Eng.Comm* 17, 6868–6877 (2015)
59. Hu, Y. S. H., Kienle, L., Guo, Y. G., Maier, J. High Lithium Electroactivity of Nanometer-Sized Rutile TiO2. *Adv. Mater.* 18, 1421–1426 (2006)

60. Reddy, M. A., Kishore, M. S., Pralong, V., Caignaert, V., Varadaraju, U. V., Raveau, B. Room Temperature Synthesis and Li Insertion into Nanocrystalline Rutile TiO2. *Electrochem. commun*. 8, 1299–1303 (2006)
61. Dylla, A. G.; Henkelman, G.; Stevenson, K. J. Lithium Insertion in Nanostructured TiO2(B) *Architectures. Acc. Chem. Res.* 46, 1104–1112 (2013)
62. (20) Ren, Y.; Liu, Z.; Pourpoint, F.; Armstrong, A. R.; Grey, C. P.; Bruce, P. G. Nanoparticulate TiO2(B): An Anode for Lithium-Ion Batteries. *Angew. Chemie - Int. Ed.* 2012, 51 (9), 2164–2167.
63. Wagemaker, M., Borghols, W. J. H. & Mulder, F. M. Large Impact of Particle Size on Insertion Reactions. A Case for Anatase Li_xTiO_2. *J. Am. Chem. Soc.* 129, 4323–4327 (2007).
64. Kavan, L., Kratochvilová, K. & Grätzel, M. Study of Nanocrystalline TiO2 (anatase) Electrode in the Accumulation Regime. *J. Electroanal. Chem.* 394, 93–102 (1995).
65. Morgan, B. J. & Watson, G. W. Role of Lithium Ordering in the LixTiO2 Anatase → Titanate Phase Transition. *J. Phys. Chem. Lett.* 2, 1657–1661 (2011).
66. De Klerk, N. J. J., Vasileiadis, A., Smith, R. B., Bazant, M. Z. & Wagemaker, M. Explaining Key Properties of Lithiation in TiO_2 Anatase Li-ion Battery Electrodes using Phase-Field Modeling. *Phys. Rev. Materials* 1, 025404 (2017).
67. Gogotsi, Y. & Penner, R. M. Energy Storage in Nanomaterials – Capacitive, Pseudocapacitive, or Battery-like? *ACS Nano* 12, 2081–2083 (2018).
68. Lindström, H., Sodergren, S., Solbrand, A., Rensmo, H., Hjelm, J., Hagfeldt, A. & Lindquist, S.-E. Li^+ Ion Insertion in TiO_2 (Anatase). 2. Voltammetry on Nanoporous Films. *J. Phys. Chem. B* 101, 7717–7722 (1997).
69. Kubiak, P., Fröschl, T., Husing, N., Hörmann, U., Kaiser, U., Schiller, R., Weiss, C. K., Landfester, K. & Wohlfahrt-Mehrens, M., TiO Anatase Nanoparticle Networks: Synthesis, Structure, and Electrochemical Performance. *Small* 7, 1690–1696 (2011).
70. Liu, Y. & Yang, Y. Recent Progress of TiO2-Based Anodes for Li Ion Batteries. *J. Nanomater.* (2016)
71. Cavallo, C., Salleo, A., Gozzi, D., Di Pascasio, F., Quaranta, S., Panetta, R., Latini, A., Solid Solutions of Rare Earth Cations in Mesoporous Anatase Beads and Their Performances in Dye-Sensitized Solar Cells. *Sci. Rep.* 5, 16785 (2015).
72. Simonarson, G., Lotsari, A., Palmqvist, A.E.C. Low Temperature Spray Deposition Synthesis of Locally Ordered Mesoporous Polycrystalline Titania Films. *Submitted* (2019)
73. Evanko, B., Yoo, J. S., Chun, S.-E., Wang, X., Ji, X., Boettcher, S. W. & Stucky, G. D. Efficient Charge Storage in Dual-Redox Electrochemical Capacitors through Reversible

Counterion-Induced Solid Complexation. *J. Am. Chem. Soc.* 138, 9373–9376 (2016).

74. L. Lutterotti, S. Matthies, and H. R. Wenk, "MAUD (Material Analysis Using Diffraction): a user friendly Java program for Rietveld texture analysis and more," in Proceedings of the 12th International Conference on Textures of Materials (ICOTOM'99), Montreal, Canada, 1, 1599, (1999).
75. Klementiev, K., Noren, K., Carlson, S., Sigfridsson Clauss, K.G.V., Persson, I. The BALDER Beamline at the MAX IV Laboratory. *J. Phys. Conf. Ser*. 712, 8-12 (2016)
76. Bard, A. J. & Faulkner, L. R. Electrochemical methods: fundamentals and applications. *Wiley* (2001).
77. Wang, J., Polleux, J., Lim, J. & Dunn, B. Pseudocapacitive Contributions to Electrochemical Energy Storage in TiO2 (Anatase) Nanoparticles. *J. Phys. Chem. C* 111, 14925–14931 (2007).
78. Henderson, G. S.; Groot, F. M. F. De; Moulton, B. J. A. X-Ray Absorption Near-Edge Structure (XANES) Spectroscopy. Rev. Mineral. Geochemistry 2014, 78, 75–138.
79. Cabaret, D.; Bordage, A.; Juhin, A.; Arfaoui, M.; Gaudry, E. First-Principles Calculations of X-Ray Absorption Spectra at the K-Edge of 3d Transition Metals: An Electronic Structure Analysis of the Pre-Edge. Phys. Chem. Chem. Phys. 2010, 12 (21), 5619–5633.
80. Luca, V.; Djajanti, S.; Howe, R. F. Structural and Electronic Properties of Sol−Gel Titanium Oxides Studied by X-Ray Absorption Spectroscopy. *J. Phys. Chem. B* 102, 10650–10657 (2002)
81. Leitzke, F. P.; Fonseca, R. O. C.; Göttlicher, J.; Steininger, R.; Jahn, S.; Prescher, C.; Lagos, M. Ti K-Edge XANES Study on the Coordination Number and Oxidation State of Titanium in Pyroxene, Olivine, Armalcolite, Ilmenite, and Silicate Glass during Mare Basalt Petrogenesis. *Contrib. to Mineral. Petrol*. 173, 1–17 (2018)
82. Jalilehvand, F. Structure of Hydrated Ions and Cyanide Complexes by X-Ray Absorption Spectroscopy, PhD. Thesis, KTH Stockholm, Sweden (2000)
83. Rehr, J. J., Ankudinov, A., Zabinsky, S. I. New Developments in NEXAFS/EXAFS Theory. *Catal. Today* 39, 263–269 (1998)
84. Qu, D. & Shi, H. Studies of Activated Carbons used in Double-Layer Capacitors. *J. Power Sources* 74, 99–107 (1998).
85. Brousse, T., Marchand, R., Taberna, P.-L. & Simon, P. TiO2 (B)/Activated Carbon Non-Aqueous Hybrid System for Energy Storage. *J. Power Sources* 158, 571–577 (2006).
86. Kim, J. H., Choi, H. J., Kim, H.-K., Lee, S.-H. & Lee, Y.-H. A Hybrid Supercapacitor Fabricated with an Activated Carbon as Cathode and an Urchin-like TiO2 as Anode. *Int. J. Hydrogen Energy* 41, 13549–13556 (2016).

87. Li, S., Wang, T., Zhu W., Lian, Y., Huang, Y., Yu, Y. Y., Qiu, J., Zhao, Y., Yong, Y. C., Li H., Controllable synthesis of uniform mesoporous H-Nb 2 O 5 /rGO nanocomposites for advanced lithium ion hybrid supercapacitors. *J. Mater. Chem. A* 7, 693–703 (2019).